Structural polymorphism of alpha-synuclein fibrils

DOCTORAL DISSERTATION

A thesis submitted in partial fulfillment of the requirements for the degree of Doctor of Philosophy

> By: Goki Tanaka

Supervisor: Dr. Nobuyuki Nukina

Graduate School of Brain Science

Doshisha University

March 2019

Kyoto, Japan

Abstract

Synucleinopathies comprise a diverse group of neurodegenerative diseases, including Parkinson disease (PD), dementia with Lewy bodies, and multiple system atrophy, which share a common pathological feature of deposition of alpha-synuclein (a-syn) in neurons or oligodendroglias. Recent findings imply that polymorphic alpha-synuclein aggregates are related to distinct pathogenesis of disease polymorphisms. However, the structural polymorphisms of alpha-synuclein fibrils are not well understood. In this thesis, we addressed structural polymorphisms of alpha-synuclein fibrils using biochemical and morphological analyses.

A-syn is highly conserved in vertebrates, and the primary sequence of mouse a-syn differs from that of humans at seven positions. However, structural differences between the aggregates formed remain to be fully characterized. Here, we studied human and mouse a-syn aggregates generated *in vitro* to analyze the structural polymorphisms of a-syn fibrils. Through the analyses of human and mouse a-syn fibrils, we found that they showed morphologically distinct amyloid fibrils with twisted and straight structures, respectively. Furthermore, we identified distinct protease-resistant core regions, long and short cores, in human and mouse a-syn aggregates, respectively. Interestingly, among the seven

unconserved amino acids, only the A53T substitution, which is one of the familial PD mutations, was responsible for this structural dimorphism. Further, we found that human a-syn seeded with A53T aggregates formed straight-type fibrils with short protease-resistant cores. These results suggest that although a-syn forms sequence-dependent distinct structures upon spontaneous aggregation, the aggregate structure becomes seed-structure-dependent upon seeding. Our human and mouse a-syn fibrils showed clearly distinct polymorphic fibrils in terms of biochemical and morphological features.

Presently, at least six disease-associated mutations in a-syn (namely A30P, E46K, H50Q, G51D, A53T, and A53E) are known to cause dominantly inherited familial forms of synucleinopathies. Therefore, we hypothesized that these disease-associated mutations induce the formation of the distinctive, alpha-synuclein polymorphic fibrils. We performed electron microscopic examination, guanidinium hydrochloride (GdnHCl) denaturation, and protease digestion to classify the aggregates from their respective point mutations as performed in a human and mouse alpha-synuclein comparison study. Using electron microscopy, we observed variations of amyloid fibrillar morphologies among the aggregates of a-syn mutants, mainly categorized into two groups: twisted fibrils, observed in both WT and E46K, and straight fibrils, observed in the other mutants. GdnHCl denaturation experiments revealed

that a-syn mutants (except E46K) were more resistant than WT to denaturation. Mass spectrometry analysis of protease-treated aggregates showed a variety of protease-resistant cores, which may correspond to their morphological properties. The difference in their properties could be associated with the clinicopathogical differences of synucleinopathies.

In this thesis, we showed that human and mouse a-syn can form distinct biochemical and morphological fibrils. The differences are regulated by a single substitution, A53T. Our seeding experiment further implied that human WT a-syn can form A53T-type structures. Based on these data, human WT a-syn can form two types of polymorphic fibrils. Our disease-associated mutation analyses imply that these two types of polymorphic fibrils are related to distinct types of synucleinopathies. Accordingly, in this thesis, our data suggest that distinct types of synucleinopathies are related to distinct types of polymorphic fibrils. In the future, we should determine the molecular structures of distinct types of fibrils and perform studies using cell or animal models to provide direct evidence for the relationship between distinct types of polymorphic fibrils and pathogenesis of synucleinopathies.

Acknowledgments

I am indebted to my supervisor, Professor Nobuyuki Nukina, for his guidance throughout the planning and execution of experiments during this research. I am grateful for his remarkable efforts dedicated towards improving my study and this manuscript. I would like to extend my gratitude to Associate Professor Tomoyuki Yamanaka for the constant support and encouragement. This thesis could never have been accomplished without his valuable efforts. I am also grateful to Assistant Professor Haruko Miyazaki for his critical suggestions and helpful advice, which came from his experience and profound comprehension of my thesis. I would also like to thank Dr. Furukawa Yoshiaki for providing the His-human and mouse vector. I thank all my considerate colleagues for their kind cooperation. Finally, I wish to extend my sincere gratitude to my family and friends for their understanding, support, and encouragement throughout my study.

Table of Contents

Chapter 1. Introduction	10
1.1. Synuleinopathies	10
1.2. Synuclein family	10
1.3. Alpha-synuclein and its aggregate formation	12
1.4. Polymorphic alpha-synuclein fibrils	17
1.5. Human and mouse alpha-synuclein	20
1.6. Disease-associated mutations of alpha-synuclein	22
Chapter 2. Materials and methods	24
Chapter 3. Results	32
3.1. Morphological and biochemical differences between human and mouse alpha-sy	nuclein
aggregates	32
3.2. A53T substitution is a main determinant for the morphological and biochemical p	roperty
of mouse alpha-synuclein aggregates.	39
3.3. Structural transmissibility of morphological and biochemical features by seeding	47
3.4. Biochemical and morphological classification of disease-associated mutant	
alpha-synuclein fibrils	57
Chapter 4. Discussion	65
4.1. Human and mouse alpha-synuclein substitution	65
4.2. Protease partial digestion and alpha-synuclein fibrils	66
4.3. Protease-resistant core and structural transmissibility of alpha-synuclein fibrils	68
4.4. Amyloid fibril polymorphisms of human and mouse alpha-synuclein based on the	
morphologies	70
4.5. Disease-associated alpha-synuclein mutations	71
4.6. Concluding remarks	75
Chanter 5 References	77

List of Figures and Tables

Figures

Fig. 1 Alpha-synuclein and its family
Fig. 2 Schematic illustration of kinetics of protein aggregation
Fig. 3 Alpha-synuclein amyloid fibrils and its molecular structure
Fig. 4 Biochemical and morphological differences in monomeric and aggregation states
between human and mouse alpha-synuclein
Fig. 5 Biochemical differences in aggregation states of human and mouse
alpha-synuclein
Fig. 6 Purified monomeric alpha-synuclein used in this study
Fig. 7 Alpha-synuclein mutants with single substitution form distinct amyloid fibrils 43
Fig. 8 Representative fibrils of human wild-type, mouse, and mutant
alpha-synuclein
Fig. 9 Proteinase K and trypsin digestion experiments show distinct patterns in human
wild-type, mouse, and mutant alpha-synuclein
Fig. 10 Alpha-synuclein mutants with single substitution form distinct proteinase K-resistant
core revealed by MALDI-TOF MS analysis
Fig. 11 Morphologies of mutation-dependent structures could be transmitted to human
wild-type alpha-synuclein by seeding reactions
Fig. 12 Representative fibrils of seed-induced fibrils of human wild-type
alpha-synuclein
Fig. 13 Proteinase K and trypsin digestion experiments show distinct patterns in seed-induced
aggregates
Fig. 14 Seed-induced aggregates show distinct proteinase K-resistant core corresponding to
the pre-formed fibril seeds
Fig. 15 AGERA reveals transmissibility of biochemical properties of
aggregates
Fig. 16 Disease-associated monomeric mutants of alpha-synuclein form distinct states 58
Fig. 17 Purified disease-associated monomeric mutants of alpha-synuclein 59
Fig. 18 Disease-associated mutations cause polymorphic aggregates of alpha-synuclein, as
observed under electron microscope
Fig. 19 Disease-associated mutations cause biochemical polymorphic aggregates of
alpha-synuclein

Fig. 20 Disease-associated mutations cause distinct proteinase K-resistant core
Tables
Table 1: List of primers used in this study
Table 2: Summary of the results
Table 3: Summary of comparisons of human wild-type and disease-associated
alpha-synuclein mutants

Abbreviations

PD: Parkinson's disease

DLB: dementia with Lewy bodies

MSA: multiple system atrophy

GCI: glial cytoplasmic inclusions

AD: Alzheimer disease

ThT: Thioflavin T fluorescence

WT: Wild-type

GdnHCl: guanidine hydrochloride

a-syn: alpha-synuclein

b-syn: beta-synuclein

g-syn: gamma-synuclein

polyacrylamide gel electrophoresis: PAGE

0.05% Tween 20/Tris-buffered saline: TBST

CBB: Coomassie Brilliant Blue

PFF: pre-formed fibrils

AGERA: agarose gel electrophoresis for resolving aggregates

EM: electron microscopy

AFM: atomic force microscopy

LB: Lewy bodies

Chapter 1. Introduction

1.1. Synucleinopathies

Synucleinopathies are a group of diverse neurodegenerative disorders that share a common pathologic lesion composed of aggregates of insoluble alpha-synuclein (a-syn) protein [1]. Lewy bodies (LB) and Lewy neurites, the pathological hallmarks of Parkinson's disease (PD) and dementia with Lewy bodies (DLB), contain filamentous forms of alpha-synucleins (a-syn) in neurons, while other neurodegenerative disorders including multiple system atrophy (MSA) also display a-syn deposits in oligodendroglia called glial cytoplasmic inclusions (GCI) [2-4]. The pathological intracellular inclusions containing a-syn in selectively vulnerable neurons and glia are linked to the onset and progression of their clinical symptoms, as well as the degeneration of affected brain regions [1, 5].

Recombinant human a-syn forms fibrillar material *in vitro* after incubation [6-8], which caused LB-like pathological hallmarks in brains of mice, rats, and marmosets several months post-injection [9, 10]. A-syn aggregates derived from the patients with MSA and PD also caused the pathological hallmarks of a-syn in mouse brain and cultures [11, 12]. These findings indicate that the a-syn aggregates must play key roles in the pathogenesis of synucleinopathies.

1.2. Synuclein family

A-syn is highly conserved throughout the vertebrates. It is composed of 140 amino acids, and is divided into three regions: amphipathic region, non-amyloid component protein, and acidic region [13] (Fig. 1A). A-syn is part of a family of proteins that also includes beta and gamma-synuclein [14]. In humans, beta-synuclein (b-syn) is 78%, and gamma-synuclein (g-syn) is 58% homologous to a-syn [15] (Fig. 1B). Despite the high homology, b-syn and g-syn fail to assemble into filaments, in keeping with the finding that antibodies directed against b-syn and g-syn do not stain the filamentous inclusions of PD, DLB, and MSA [3, 16]. On the other hand, a case-control study indicated that not only SNCA (a-syn gene), but also SNCG (g-syn gene), affect the risk of developing diffuse Lewy body diseases [17]. Cerebellar spinal fluid a-syn, b-syn, and g-syn concentrations were found to be increased in Alzheimer and Creutzfeldt-Jakob disease but were found to remain unchanged in PD, PD dementia, DLB and atypical parkinsonian syndromes using multiple reaction monitoring mass spectrometry [18]. Despite the lower tendencies of aggregation formation, some reports suggest that b-syn and g-syn play important roles in the progression of neurodegeneration and dementia, as shown in mouse models [19, 20]. These findings suggested that b-syn and g-syn might affect the progression of neurodegenerative diseases. However, the relationship between them and the clinical phenotypes remain elusive, because unlike a-syn, b-syn and

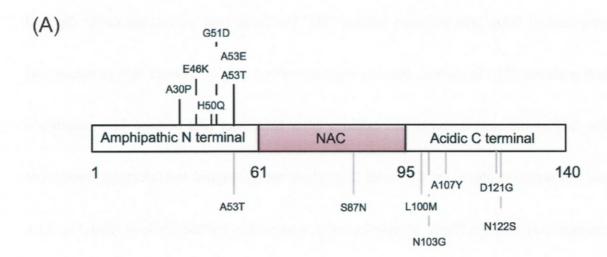
g-syn are not found in the brains of patients with PD, DLB, and MSA. Therefore, compared with b-syn and g-syn, a-syn is considered the most important protein in the pathogenesis of synucleinopathies.

1.3. Alpha-synuclein and its aggregate formation

The kinetics of a-syn aggregation follows a nucleation-dependent process, where monomers initially form oligomeric species inducing the final formation of the amyloid fibrillar aggregates (Fig. 2) [21, 22]. On the other hand, another aggregation process, seeding, is a simple aggregation process, in which the presence of pre-formed fibrils, termed "seed", facilitate the formation of fibrillar aggregates by eliminating the need for primary nucleation (Fig. 2) [23]. Both aggregation processes are important when focusing on the disease progression of synucleinopathies, and both phenomena can be directly observed not only *in vitro*, but also in cell assay systems [24]. Importantly, amyloidgenic proteins including a-syn can form amyloid fibrils, which have common structure regardless of the aggregation process.

Morphologically, mature fibrillar forms of soluble protein are typically formed by two or more elementary protofilaments around ~5 nm in width, which can be clearly observed using electron microscopy (Fig. 3A) [25-27]. Structurally, the fibrils are commonly

composed of fuzzy coat and core regions [28]. The fuzzy coat regions are easily digested with proteases [28]. In contrast, the core regions cannot be easily digested with proteases [28]. The fold of the core is sometimes called a cross beta-sheet fold because beta-strands are oriented perpendicular to the fibril axis [29]. These morphological and structural features are common even in a-syn fibrils. Morphologically, a-syn easily formed fibrils in vitro (Fig. 3A). The core structure of a-syn fibril showed hydrogen bonds in register along the fibril axis (core region), which is orthogonal to the hydrogen bond geometry in a standard Greek-key motif from residues 44 to 96 (Fig. 3B and 3D) [25, 30]. X-ray fiber diffraction patterns in fibrils of a-syn exhibited the archetypal amyloid meridional diffraction at 4.7-4.9 Å, indicating that a-syn fibrils formed a cross-β structure (Fig. 3D) [25]. Residues 50-57, containing three of the mutation sites associated with familial synucleinopathies, form the interface between the two protofilaments and contribute to a-syn fibril stability (Fig. 3C) [31]. Amyloid fibrils, which are formed by a-syn are essential in synucleinopathies, though their pathological role remains unclear. Besides, although subsets of in vitro experiments revealed that a-syn forms amyloid fibrils, how different synucleinopathies progress despite the common deposition of a-syn aggregates remains unknown.



(B)

alpha-synuclein	MDVFMKGLSKAKEGVVAAAEKTKQGVAE	AAGKTKEGVLYVGSKTKEGVVHGVATVAEKTK	60
beta-synuclein	MDVFMKGLSMAKEGVVAAAEKTKQGVTE	AAEKTKEGVLYVGSKTREGVVQGVASVAEKTK	60
gamma-synuclein	MDVFKKGFSIAKEGVVGAVÉKTKQGVTE	AAEKTKEGVMYVGAKTKENVVQSVTSVAEKTK	60
alpha-synuclein	EQVTNVGGAVVTGVTAVAQKTVEGAGSI.	AAATGFVKKDQLGKNEEGAP-QEGILE	114
beta-synuclein	EQASHLGGAVFSGAGNI	AAATGLVKREEFPTDLKPEEVAQEA-AEEPLI	108
gamma-synuclein	EQANAVSEAVVSSVNTVATKTVEEAENI.	AVTSGVVRKEDLRPSAPQQEGEASKEKEEVAE	120
alpha-synuclein	DMPVDPDNEAYEMPSEEGYQDYEPEA	140	
beta-synuclein	EPLMEPEGESYEDPPQEEYQEYEPEA	134 (78%)	
gamma-synuclein	EAQSGGD	127 (58%)	

Fig. 1 Alpha-synuclein and its family

(A) Schematic illustration of the human WT a-syn, comprising three distinct domains (amphipathic N-terminal, NAC, and acidic C-terminal). Disease-associated mutations of a-syn are located in the amphipathic N-terminal regions (A30P, E46K, H50Q, G51D, A53T, and A53E), shown with black lines. Sequence comparison for human and mouse a-syn are shown under the a-syn (A53T, S87N, L100M, N103G, A107Y, D121G, and N122S) with gray lines. (B) Alignment of the primary amino acid sequences of synucleins. The amino acids residues different from that in a-syn are shown in red color. The homologies to a-syn are shown in the parenthesis on the right, which is based on a previous article [15]. The schematic illustration in (A) is based on a previous article [32].

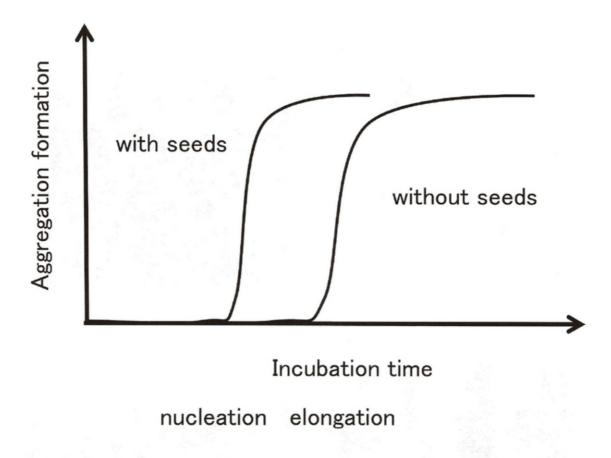


Fig. 2 Schematic illustration of kinetics of protein aggregation

The a-syn protein forms aggregates under *in vitro* conditions. Basically, monomeric protein forms an oligomeric species, which is called the nucleation process. Then, the oligomeric form binds further monomeric proteins, forming fibrillar aggregates, which is called the elongation process. With pre-formed fibril seeds in protein solutions, the proteins form fibrillar aggregates based on seeds without nucleation process. The schematic illustration is based on previous reports [21, 23]

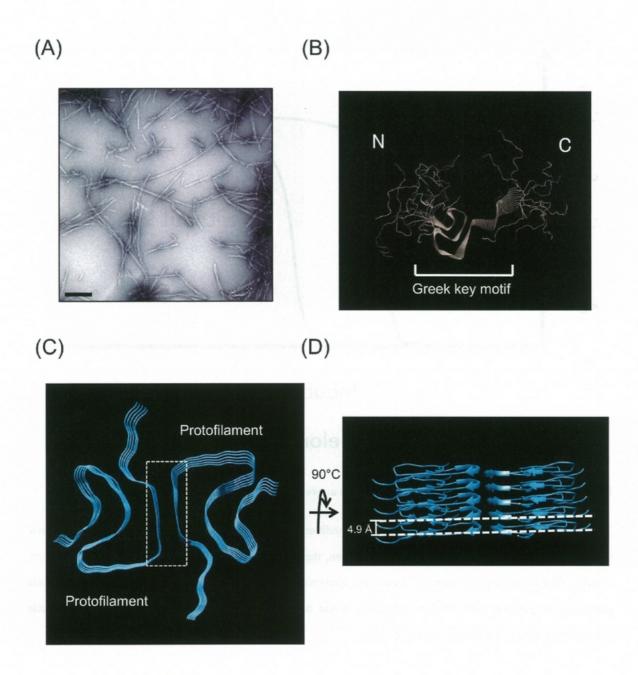


Fig. 3 Alpha-synuclein amyloid fibrils and its molecular structure

(A) Typically, amyloid fibrils derived from human WT a-syn formed under *in vitro* conditions. Scale bar shows 200 nm. Molecular structures of a-syn amyloid fibrils (PDB entry 2n0a (B) and PDB entry 6flt (C, D)) are shown. N and C indicate the N and C terminal region, respectively. NAC region forms the Greek key motif (B). Single fibrils of a-syn are formed by two protofilaments of a-syn (C), which are highly stacked along the fibril axis per 4.9 Å (D). The area related to the fibril stability (residues 50-57) is enclosed by dotted lines. The molecular structure models of a-syn have been taken from previous articles [25, 31].

1.4. Polymorphic alpha-synuclein fibrils

Recent studies demonstrate that MSA is unequivocally caused by a-syn aggregates, which are misfolded proteins that undergo self-propagation and are capable of transmitting disease pathology in transgenic mice or cultured cells [12, 33-35]. However, PD, PD with dementia, and DLB transmission studies have been unsuccessful [12, 34]. Another recent report clearly showed that pathological a-syn aggregates in GCIs and LB show a characteristic conformation and are biologically distinct [36]. These recent reports suggest that distinct conformations of misfolded a-syn aggregates may be responsible for these diseases. Besides, distinct a-syn aggregates generated in vitro display differential seeding capacities, inducing conformation-specific pathology and neurotoxic phenotypes in rodent [37-39]. Particularly, the conformational differences between distinct a-syn aggregates seemed to be highly related with the disease polymorphisms of synucleinopathy. Thus, analysis of the conformational differences in a-syn polymorphic fibrils might help to elucidate the pathological distinctiveness of synucleinopathies.

Despite its importance, studies on conformational differences in amyloid fibrils of a-syn are quite limited. Morphology of polymorphic amyloid fibrils is mainly investigated by atomic force microscopy (AFM) and electron microscopy (EM). Different salt conditions

induce distinct polymorphic aggregates: fibrils (constant width 13 nm) and ribbons (wide: 18 nm and narrow: 8 nm) determined by EM [40]. Using a fluorescent dye, Thioflavin T (ThT), which reacts with beta-sheet formation, other groups have reported two types of amyloid fibrils, helical (periodicity: 74 ± 6 nm, height: 5.7 nm) and ribbon-like (height: 6.3 nm), observed by AFM [41]. Genetic factors, such as disease-associated mutations, also affect the fibril states of a-syn [42]. These reports imply that morphologically distinct types of fibrils are easily formed under distinct *in vitro* conditions or genetic manipulations of a-syn.

Although the morphological distinctiveness of the a-syn fibrils are widely known, it was unclear how these morphologically distinct fibrils form distinct conformational structures. Based on the structure of a-syn fibrils, it is assumed that fuzzy coat and/or core regions are distinct. Recent analyses using cryo-EM provided new insights into the structural differences in polymorphic a-syn fibrils. Their structural data indicated that two morphologically distinct types of fibrils, twister and rod, are induced by distinct protofilament packing in the core region [43].

Because fuzzy coat regions are easily digested with proteases, protease partial digestion experiments have been performed to analyze the states of fuzzy coat regions in fibrillar aggregates. In the case of a-syn fibrils, protease partial digestion experiments

prominently reflected the polymorphisms of aggregates [36, 38, 42]. A previous study demonstrated that the N-terminus contributes to the distinct formations of a-syn amyloid fibrils (e.g., helical and ribbon-like) [41]. Another study reported that truncation of C-terminal region enhanced formation of twisted or shorter a-syn amyloid fibrils [44]. Nevertheless, the molecular structure of fuzzy coat regions in a-syn fibrils remains elusive, because of the dynamic nature of the fuzzy coat regions. Collectively, these findings suggest that both core region and fuzzy coat region seem to contribute to the morphologically different types of a-syn fibrils. However, as yet, the simultaneous detection of the core, the fuzzy coat region and the morphological distinctiveness of a-syn fibrils has not been successful. Therefore, it is unclear how the morphologies are related with the structural differences. In this thesis, the relationship between the structural differences of the different regions with the morphologically distinct a-syn fibrils are elucidated.

To address the polymorphisms of a-syn fibrils, we tackled three main challenges.

First, we aimed to obtain the polymorphic aggregates of a-syn. Because a-syn easily forms distinct fibrils under distinct *in vitro* conditions, we carefully considered and optimized the conditions to obtain the different types of fibrils. Second, we evaluated the available methods for analysis of aggregate states and identified the best method to analyze the polymorphism

of a-syn fibrils. Finally, we investigated the properties of the polymorphic fibrils with an aim to elucidate the relationship between the polymorphisms of human a-syn fibrils and the pathogenicity of synucleinopathies.

To obtain the polymorphic fibrils, we first determined the differences between human and mouse a-syn (See details in 1.5. Human and mouse alpha-synuclein). To analyze the polymorphic fibrils and uncover its properties, biochemical and morphological analyses were carried out, including EM analysis, protease partial digestion, and protease-resistant core analyses with mass spectrometry. These methods could clarify the properties of polymorphic fibrils. To investigate the relationships between the properties of the polymorphic fibrils and pathogenicity of synucleinopathies, we analyzed the disease-mutant a-syn fibrils (See details 1.6. Disease-associated mutations of alpha-synuclein).

1.5. Human and mouse alpha-synuclein

The SNCA gene of mouse encodes mouse a-syn containing substitutions at position 53, 87, 100, 103, 107, 121, and 122 when compared with human a-syn (Fig. 1A). In vivo assessment of seeding a-syn aggregates derived from human diseases into mouse brains is relevant for determining the species barriers as reported for prion disease [45-47]. The

cross-species seeding of human a-syn aggregates attenuate propagation and spreading of aggregates in mice brain [48-50]. Using chimeric a-syn fibrils, it was reported that interspecies substitution of human a-syn residues with the mouse a-syn residues at A53 to T and S87 to N resulted in a higher seeding efficiency than obtained with human WT a-syn seeds both *in vitro* and *in vivo* [51]. These findings imply that the human and mouse a-syns are biologically distinct. Cell-free *in vitro* analyses of human and mouse a-syn further indicated that these two a-syn fibrils show distinct conformations, which are regulated by the two substitutions A53T and S87N [51-54]. These observations imply that human and mouse a-syn are biologically distinct and show unique conformations. Therefore, we used human and mouse a-syn to analyze the properties of polymorphic fibrils.

Because the amino acid composition of rodent a-syn differs from that of human a-syn, which yielded ambiguous results for fibril conformation, the conformation of the polymorphic a-syn fibrils could not be directly connected with the neurotoxicity and pathogenicity in rodents. Thus, the investigation of the differences between human and mouse a-syn itself is important to uncover the pathogenic contributions of a-syn fibril structures to synucleinopathies.

1.6. Disease-associated mutations of alpha-synuclein

In addition to the difference between human and mouse a-syn, this work focused on the disease-associated mutations and the relationship between the properties of polymorphic fibrils and the pathogenicity of synucleinopathies. Six missense mutations (A30P, E46K, H50Q, G51D, A53T, and A53E) in the a-syn (SNCA) gene have been reported to cause dominantly-inherited familial synucleinopathies; E46K causes DLB, A30P and H50Q cause classic PD, and G51D, A53T, and A53E cause severe PD, sometimes with MSA features [55-59] (Fig. 1A). These mutations have been shown to differentially modulate a-syn aggregation propensity in vitro [60]. For example, the secondary structure of A53T and E46K aggregates shows differences compared with that of WT, as revealed by solid-state NMR [61]. Therefore, disease-associated mutants of a-syn form distinct aggregates relative to WT aggregates. However, since novel subsets of disease-associated mutations have been discovered in the past 5 years (H50Q; 2013 [62], G51D; 2013 [58], A53E; 2014 [59]), and a variety of synucleinopathies have been identified, studies on the evaluation of biochemical properties of disease-associated a-syn aggregates would be highly significant.

In this thesis, as mentioned above, we studied the difference between human and mouse a-syn using recombinant protein expression system purified from *Escherichia coli*. Based on previous studies, we hypothesized that human and mouse a-syn form distinct polymorphic fibrils and may be explained by single interspecies substitutions. A single substitution experiment can contribute to elucidate the responsible amino acids for the different properties between human and mouse a-syn fibrils. Further, to discuss the relationship between the properties of polymorphic fibrils and clinical and pathological phenotypes of synucleinopathy, we analyzed disease-associated mutant a-syn aggregates.

Chapter 2. Material and Methods

Purification of recombinant alpha-synuclein: Plasmids pET 15b encoding His-human a-syn and His-mouse a-syn were described previously [50]. Introduction of mutations was performed through Inverse PCR using a KOD neo DNA polymerase (Toyobo) and confirmed by DNA sequencing. The primers used in this study are listed in Supplementary Table 1. All mutants were established by site directed mutation of codon 136 (TAC to TAT), which avoids mis-incorporation of Cys at this position [63]. All data obtained with TAC mutants are shown in Supplementary Fig. S2-S5. The E. coli strain BL21 (DE3) was transformed with the expression vector pET15b, encoding a-syn and cultured at 37 °C for several hours and 0.5 M isopropyl 1-thio-β-D-galactopyranoside was added and cultured further for 6 h. To extract proteins from E. coli, the cells were lysed with phosphate-buffered saline containing 2% Triton X-100. After sonication and centrifugation, the supernatant was immediately poured into a 15-mL centrifuge tube containing Ni-sepharose beads (GE Healthcare), then rotated for 1 h at 4 °C. The beads were washed twice with 50 mM Tris, 100 mM NaCl, 30 mM imidazole, pH 8.0, after which a-syn was eluted with 50 mM Tris, 100 mM NaCl, 250 mM imidazole, pH 8.0. The eluted samples were filtered using 0.22-µm filter (Millex) to obtain pure protein, and concentrated by Vivaspin Turbo15 (Sartorius). The His-tag was cleaved by Thrombin agarose (Sigma) at 25 °C for 20 h. To eliminate Thrombin agarose, the solution was centrifuged at 15,000 rpm for 3 min; then, the supernatant was filtrated with a 0.22-μm filter. A-syn protein concentration was determined from the absorption at 280 nm in the presence of 6 M guanidine hydrochloride by using 5690 M⁻¹ cm⁻¹ or 7450 M⁻¹ cm⁻¹ as extinction coefficient. The samples obtained were used for making aggregates.

Gel electrophoresis: To evaluate the monomeric state of a-syn, we performed native-polyacrylamide gel electrophoresis (PAGE). For native-PAGE, 2.5 μL of 100 μM purified a-syn was mixed with 17.5 μL of sample buffer (100 mM Tris-HCl pH 6.8, 20% glycerol, and 0.01% bromophenol blue). Electrophoresis was performed in 12 or 15% polyacrylamide gels (6.25% stacking gel)) at 20-30 mA for 30–60 min at room temperature with running buffer (100 mM Tris, 100 mM glycine).

For SDS-PAGE, samples were mixed with SDS-containing Laemmli buffer (100 mM Tris-HCl, pH 6.8, 4% SDS, 2% 2-mercaptoethanol, 20% glycerol, and 0.01% bromophenol blue). Electrophoresis was performed in 12 or 15% (w/v) SDS-containing polyacrylamide gels (6.25% stacking gel) at 20 mA for 60–120 min at room temperature with running buffer (100 mM Tris, 100 mM glycine, and 0.1% SDS). Boiled samples (10-15 μL)

were loaded into the gel. The gels were later stained with Coomassie Brilliant Blue (CBB).

AGERA (agarose gel electrophoresis for resolving aggregates) was performed as previously described [64]. Agarose (1%) resolved in gel buffer (100 mM Tris and 100 mM glycine) was prepared. The samples were mixed with SDS-containing Laemmli buffer, and without boiling, were loaded into the gel. Electrophoresis was performed, using an apparatus for PAGEL (ATTO), at 20-30 mA for 30-60 min at room temperature with running buffer (100 mM Tris, 100 mM glycine, and 0.1% SDS). The gels were used for western blotting.

Western blotting: For western blot analysis, proteins in the gels were transferred onto a PVDF membrane for 90 (AGERA) min at 150 mA at room temperature. The membranes were blocked using 5% skim milk in 0.05% Tween 20/Tris-buffered saline (TBST) and incubated with primary antibody overnight at 4 °C. Primary antibody for a-syn (S1) was described previously [65]. Then, the membranes were washed three times in TBST and incubated for 1 h with horseradish peroxidase-conjugated secondary antibody (dilution 1:1,000). Immunoreactive proteins were detected with enhanced chemiluminescence reagent, Luminata (Millipore). Chemiluminescent signals were obtained using ImageQuant LAS-4000 (GE Healthcare).

Electron microscopy: Morphological observations of a-syn fibrils were done using an electron microscope H-7000 (Hitachi) at an accelerating voltage of 100 kV. The samples were adsorbed on 400-mesh grids coated by a glow-charged supporting amorphous carbon film and negatively stained with 2% uranyl acetate. The images were recorded on the Orius CCD camera (Gatan) and the width of a fibrillar structure was measured using ImageJ. The means of the number of fibrils were counted from electron micrographs of three different fields of view for each sample.

In vitro aggregation: Purified a-syn monomers (100 μ M, 150 μ L) were placed in a Cute Mixer CM-1000 (Tokyo Rikakikai) with buffer A (pH 8.0) and plastic beads (Sanplatec) and incubated at 37 °C in an incubator, with shaking at 1,000 rpm, for 7 days. Aggregates were pelleted by spinning at 50,000 rpm for 20 min, re-suspended in buffer A (150 μ L) and then sonicated using Bioruptor (Biorad). These aggregates were used for experiments as pre-formed fibrils (PFF). To perform a seeding reaction, 7.5 μ L (5%) of PFF was added to monomeric forms of a-syn (100 μ M) in 142.5 μ L of buffer A and incubated. The obtained seed-induced aggregates were used for experiments.

Protease partial digestion of aggregates: Partial digestion with proteases was performed based on a previous study [40]. Briefly, obtained a-syn aggregates in buffer A were treated with 4 μg/mL proteinase K (Nacalai) or 40 μg/mL trypsin (Promega). Aliquots were transferred at different time intervals (20, 60, 120, 180, 240, and 300 s) into Eppendorf tubes and treated with the sample buffer for 10 min at 90 °C (proteinase K) or at –80 °C (trypsin) to immediately arrest the cleavage reaction. The samples were subjected to SDS-PAGE to monitor the time course of a-syn cleavage. The gels were stained with CBB and the signals were obtained using ImageQuant LAS-4000 (GE Healthcare).

Mass spectral analysis of amyloid cores: A-syn aggregates were treated with proteinase K (4 μg/mL) for 120 min for amyloid core analysis at 37 °C, based on a previous report [66]. Protease-resistant amyloid fibrils were collected by ultracentrifugation (50,000 rpm for 20 min), and the pellets were dissolved in 6 M guanidine hydrochloride (GdnHCl), 10 mM Tris·HCl (pH 8.0). The dissociated amyloid fibril peptides were desalted using self-made C18 (3M Empore solid phase extraction disk) Stage Tip and analyzed by MALDI-TOF MS (autoflex speed TOF/TOF, Bruker Daltonics).

Thermal denaturation: Equal amounts of protein (100 μM) in buffer A were mixed with an excess of SYPRO Orange (100× in DMSO, Sigma) to a volume of 20 μL and added into a 96-well plate, followed by measurement of fluorescence, expressed in arbitrary units (a.u.), using the LightCycler 480 (Roche). Thermal denaturation experiments were conducted at a heating rate of 0.06 °C/s (from 20–90 °C). The continuous acquisition mode was used during the protein melting reaction Obtained data were normalized by each value at 20 °C.

Thioflavin T fluorescence: In a 96-well plate, 2.5 μ L of α -synuclein aggregates were mixed with 25 μ M ThT in 100 μ L buffer A. Fluorescence was measured in a plate reader (Perkin Elmer) with an excitation filter (430–442 nm cutoff) and an emission filter (485 nm cutoff).

GdnHCl denaturation assay: GdnHCl buffer (GdnHCl, 100 mM Tris-HCl at pH 8.0) was prepared at different concentrations (GdnHCl 0–6 M). Obtained aggregates (2.5 μL) were mixed into 2.5 μL of each concentration of GdnHCl buffer in a PCR tube for 1 h at room temperature, followed by measurement of ThT fluorescence via Envision (Perkin Elmer). The fluorescence data were normalized using values from samples without any added GdnHCl.

Statistical analysis: For comparison between two sample groups, data were first analyzed by t-test. Difference between comparisons was considered to be significant when P < 0.05.

Table 1. List of primers used in this study

Mutation		Primer (5'- 3')
V to TAT	Forward	GAAGGGTATCAAGACTATGAACCTGAAGCCTAA
Y to TAT	Reverse	TTAGGCTTCAGGTTCATAGTCTTGATACCCTTC
A30P	Forward	GGTGTGGCAGAAGCACCAGGAAAGACAAAAGAG
	Reverse	CTCTTTTGTCTTTCCTGGTGCTTCTGCCACACC
E46K	Forward	GGCTCCAAAACCAAGAAGGGAGTGGTGCATGGT
	Reverse	ACCATGCACCACTCCCTTCTTGGTTTTGGAGCC
H50Q	Forward	AAGGAGGAGTGGCAAGGTGTGGCAACAGTG
	Reverse	CACTGTTGCCACACCTTGCACCACTCCCTCCTT
0545	Forward	GAGGGAGTGGTGCATGTGGCAACAGTGGCT
G51D	Reverse	AGCCACTGTTGCCACATCATGCACCACTCCCTC
AFOT	Forward	GTGGTGCATGGTGTGACAACAGTGGCTGAGAAG
A53T	Reverse	CTTCTCAGCCACTGTTGTCACACCATGCACCAC
A53E	Forward	GTGGTGCATGGTGTGGAAACAGTGGCTGAGAAG
	Reverse	CTTCTCAGCCACTGTTTCCACACCATGCACCAC
0071	Forward	GTGGAGGGAGCAGCAGCCACT
S87N	Reverse	AGTGGCTGCAATGTTCCCTGCTCCCTCCAC
1.40084	Forward	GTCAAAAAGGACCAGATGGGCAAGAATGAAGAA
L100M	Reverse	TTCTTCATTCTTGCCCATCTGGTCCTTTTTGAC
NAOSC	Forward	GACCAGTTGGGCAAGGTGAAGAAGGAGCCCCA
N103G	Reverse	TGGGGCTCCTTCTCACCCTTGCCCAACTGGTC
A4077/	Forward	AAGAATGAAGAAGGATATCCACAGGAAGGAATT
A107Y	Reverse	AATTCCTTCCTGTGGATATCCTTCTTCATTCTT
D4240	Forward	ATGCCTGTGGATCCTGGCAATGAGGCTTATGAA
D121G	Reverse	TTCATAAGCCTCATTGCCAGGATCCACAGGCAT
NACCO	Forward	CCTGTGGATCCTGACAGTGAGGCTTATGAAATG
N122S	Reverse	CATTTCATAAGCCTCACTGTCAGGATCCACAGG

Chapter 3. Results

3.1. Morphological and biochemical differences between human and mouse alpha-synuclein aggregates

The substitutions between human and mouse a-syn are distributed unevenly along the sequence; one (A53T) in the N-terminal region, one (S87N) in the NAC region and five (L100M, N103G, A107Y, D121G and N122S) in the C terminal region (Fig. 4A) [52]. Human and mouse a-syn proteins were analyzed by native-PAGE in order to examine the state of a-syn after purification from *E. coli*. Although we detected strong single band in CBB-stained SDS-PAGE (Fig. 5), a mobility difference between human and mouse a-syn was observed in native-PAGE (Fig. 4B), probably reflecting the charge differences between these proteins.

To test whether the amino acid differences alter the structural properties of the aggregates, we compared morphologies of human and mouse a-syn aggregates by EM observation and found distinct morphologies. Human a-syn formed twisted fibrils with a width that varied between 12.68 ± 2.09 nm and 21.05 ± 2.57 nm and displayed a periodicity of ~110 nm (n = 10) (Fig. 4C). In contrast, the mouse a-syn fibrils were straight with a width of 15.36 ± 1.62 nm (n = 10) (Fig. 4D). Further, the cross-over points were difficult to identify

in mouse straight type fibrils. To examine the homogeneity of polymorphic fibrils, we counted the number of each fibril, and confirmed that human and mouse a-syn formed almost homogenous populations of distinct types of fibrils (twisted, 100% and straight, 97.52%, respectively). These results suggested that human and mouse a-syn formed morphologically distinct fibrils *in vitro*.

Previous reports showed the existence of two types (straight and twisted) of fibrils for each mouse or human a-syn fibrils [52, 67] and proposed that the different fibril morphologies arise due to different reaction conditions [68]. However, the current study clearly showed the homogenous morphology of human a-syn fibrils (twisted) and mouse a-syn fibrils (straight). The difference in the observed results may be because the a-syn used in this study utilized codon136 mutant (TAC to TAT), which avoids mis-incorporation of Cys at this position in *E. coli* and produces a single a-syn Y136. Non-mutant a-syn, which may have been used in the previous studies, produces two types of a-syn including Y136 and C136 [63]. Therefore, although we do not rule out the reaction conditions in the previous studies, the presence of non-mutant a-syn might explain the production of different types of fibrils [67].

Partial digestion with various proteases has been used to reveal the biochemical

properties of different a-syn fibrils [51]. Similarly, we performed partial digestion with proteases to identify the difference between human and mouse a-syn fibrils. Proteinase K treatment showed slower digestion of human a-syn compared with the rapid digestion of mouse a-syn fibrils (Fig. 5A and Supplementary Fig. S2), consistent with previous report [51]. To analyze the precise differences in the digestion patterns, we performed quantification of the intensity of bands digested with proteinase K (4 µg/mL, Supplementary Fig. S3; 1 µg/mL, Supplementary Fig. S4). We detected 4 bands during partial digestion with proteinase K (Supplementary Fig. S2), which showed distinct digestion patterns in addition to significant differences in the digestion rate. The 2nd band in human a-syn showed resistance to digestion with proteinase K compared with that of the mouse a-syn. In contrast, the 3rd and 4th bands appeared earlier in mouse a-syn digestion samples than in the human a-syn samples. The distinct patterns and digestion rates in bands detected with 4 µg/mL proteinase K were similar to that observed with 1 µg/mL proteinase K (Supplementary Fig. S4). Additionally, we confirmed that the distinct digestion patterns were not detected in monomeric states of human and mouse a-syn (Supplementary Fig. S2D). To further clarify the digestion patterns, we used another protease, trypsin. Trypsin digestion revealed additional differences between human a-syn and mouse a-syn fibrils (Fig. 5B and Supplementary Fig. S5). We observed

different number of bands during partial digestion with two different concentrations of trypsin (human: 2 bands, mouse: 3 bands at 20 s). Quantification of the intensity of bands obtained after digestion with trypsin (40 µg/mL, Supplementary Fig. S5E; 10 µg/mL, Supplementary Fig. S5F) indicated that the 1st band of mouse a-syn fibrils was significantly decreased as compared with that of human a-syn; this was consistent with that observed after digestion with proteinase K. Additionally, we confirmed that the distinct digestion patterns after trypsin treatment could not be detected in monomeric states of human and mouse a-syn (Supplementary Fig. S2D). Thus, the protease partial digestion experiment clarified the distinctiveness of fibrillar states of human and mouse a-syn. Next, we further analyzed biochemical properties of human and mouse a-syn fibrils by detecting the states of denaturation by GdnHCl. The states of denaturation were evaluated using ThT, a small molecule that produces a strong fluorescence upon binding to amyloid fibrils. Comparison of the curves obtained by denaturation with GdnHCl for human and mouse a-syn fibrils showed that the curve for mouse a-syn fibrils was to the right of that for human a-syn fibrils (Supplementary Fig. S6A). Moreover, the values for denaturation by 1.5 M GdnHCl were significantly higher for mouse a-syn fibrils than for human a-syn fibrils (Supplementary Fig. S6B). These results implied that mouse a-syn fibrils had higher resistance to denaturation by

GdnHCl. Taken together, the biochemical analyses clearly suggested that human and mouse a-syn fibrils have distinct biochemical properties.

In general, protein fibrillar aggregates are composed of a protease-resistant "core" and an associated "fuzzy coat", which is susceptible to proteolysis [28]. Next, an attempt was made to identify which region of an a-syn forms the protease-resistant core of the aggregate. A-syn aggregates were digested with the nonspecific protease, proteinase K, to obtain proteinase K-resistant core of a-syn fibrils [69, 70]. MALDI-TOF mass spectrometry analysis of human a-syn amyloid core regions revealed peaks at mainly m/z 9127.1, m/z 9539.4, and m/z 10914.7 in the spectra of digested human a-syn fibrils (the long cores) (Fig. 5C). In contrast, the peak for the protease-resistant fragment of mouse a-syn fibrils was mainly detected at m/z 7978.6 (the short core). These results revealed that the human and mouse a-syn fibrils contain different core regions and further supports the structural polymorphism of amyloid fibrils. Taken together, we conclude that human and mouse a-syn form morphologically and biochemically distinct amyloid fibrils.

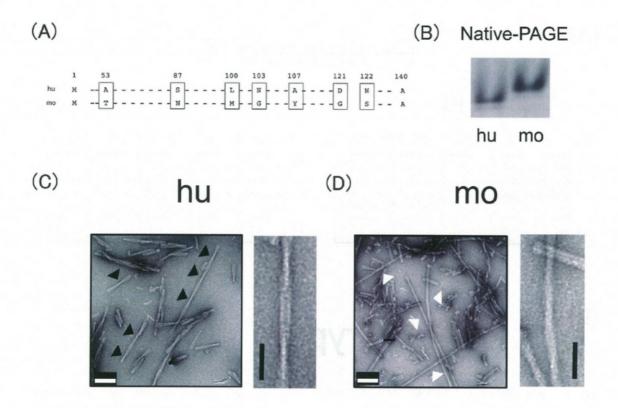
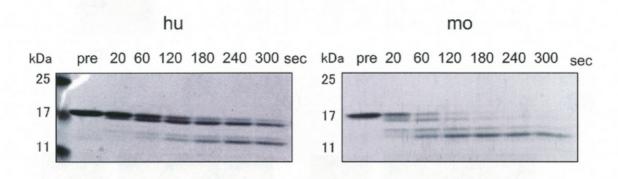


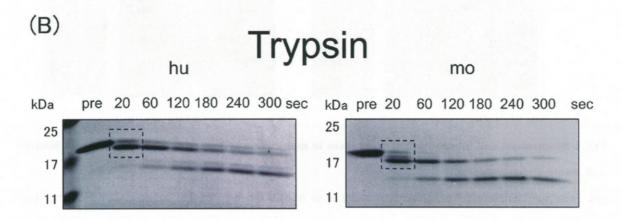
Fig. 4 Biochemical and morphological differences in monomeric and aggregation states between human and mouse alpha-synuclein

(A) Sequence comparison for human (hu) and mouse (mo) a-syn highlighting amino acid differences. (B) Native-PAGE data of human and mouse a-syn. The gel was stained with CBB. (C, D) Electron micrographs of human and mouse a-syn aggregates. Black and white arrowheads indicate (C) twisted sites and (D) straight fibrils, respectively. Representative fibrils are shown on the right side of each electron micrograph. (C) Human a-syn forms twisted fibrils (twisted) that have wide and narrow segments while (D) mouse a-syn forms straight type fibrils (straight), which does not have clear periodicity. Black and white scale bars show 50 nm and 100 nm, respectively.

(A)

Proteinase K





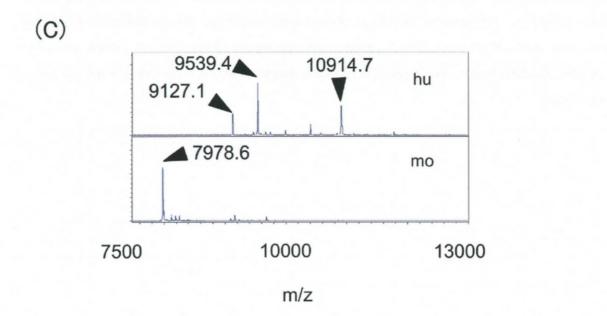


Fig. 5 Biochemical differences in aggregation states of human and mouse alpha-synuclein

Protease partial digestions with (A) proteinase K or (B) trypsin. Pre indicates pre-digested samples. Each number indicates reaction times in seconds (sec). The digestion patterns at 20 s by trypsin are shown in dotted squares to visualize the difference in the number of bands (human: 2 bands, mouse: 3 bands). More details are shown in Supplementary Fig. S2-S5. (C) MALDI-TOF MS spectra (m/z 7500–13,000) of core peptides derived from human and mouse a-syn aggregates. Observed mass is shown in each spectrum. Human and mouse a-syn aggregates are formed by long core (m/z 9127.1, m/z 9539.4, m/z 10914.7) and short core (m/z 7978.6), respectively.

3.2. A53T substitution is a main determinant for the morphological and biochemical property of mouse alpha-synuclein aggregates

To identify the amino acid(s) responsible for the structural differences between human and mouse a-syn fibrils, we generated the mutants of human a-syn, each containing a substitution of the amino acids different between human and mouse a-syn. We performed SDS-PAGE and native-PAGE analysis for these mutants (Fig. 6). As shown in Fig. 6A, D121G migrated similar to that of mouse a-syn in native-PAGE, clearly indicating that D121, with its negatively charged aspartate, was responsible for the electrophoretic mobility difference between human and mouse a-syn.

All seven point-mutants of human a-syn formed amyloid fibrils *in vitro* under our experimental conditions (Fig. 7). Typically, human a-syn mutants substituted with S87N, L100M, and N122S (Group A) predominantly formed twisted type of fibrils (Fig. 7A, 7C, 7D,

and 7H). In contrast, A53T formed straight type of fibrils (Group B) as observed in mouse a-syn (Fig. 7B and 7I). However, N103G, A107Y, and D121G showed both twisted and bundles of straight fibrils (Group C) (Fig. 7E, 7F, and 7G). Representative fibrils are shown in Fig. 8. The morphological analysis using EM suggests that a-syn fibrils show mutation-dependent structural polymorphism.

When comparing the proteinase K partial digestion pattern of fibrils derived from the mutants, they did not correspond to the fibrillar morphology (Fig. 9). N122S showed digestion patterns similar to mouse patterns, although the predominant morphology in N122S was of the twisted type. Similarly, the trypsin partial digestion pattern showed inconsistencies with the morphology (Fig. 9B).

We further examined the protease resistant core of mutant a-syn fibrils (Fig. 10). The long cores of human a-syn fibrils are designated as a (m/z 9127.1), b (m/z 9539.4), and c (m/z 10914.7). The presence of a, b, c signals in S87N, L100M, N103G, A107Y, D121G, and N122S mutants were observed (Group A and Group C), although the rates of intensity were distinct. Despite the similar morphologies, N103G and A107Y showed distinct spectral intensities. In contrast, the short core of mouse type (designated as d (m/z 7900.4), e (m/z 8312.7)) was observed in A53T in the spectra (Group B). A107Y and D121G also included

the short core peak(s), though the intensities were relatively low. The minor differences in the peaks (a, b, c, d, and e) between human WT a-syn and mutants or between mouse a-syn and A53T were observed because the mass shifts were caused by amino acid substitutions.

Although the partial digestion patterns with proteases only partially corresponded to the shape of amyloid fibrils, the protease-resistant cores were highly consistent with distinct morphologies of amyloid fibrils (twisted and twisted with bundles; long core, straight; short core). These results, for the first time, showed that the interspecies single substitutions used in this study could regulate distinct biochemical properties in different mutant a-syn aggregates. Additionally, focusing on the difference between human and mouse a-syn aggregates (Fig. 4 and 5), the results strongly suggested that a single substitution of A53T mainly regulated the morphological and biochemical differences.

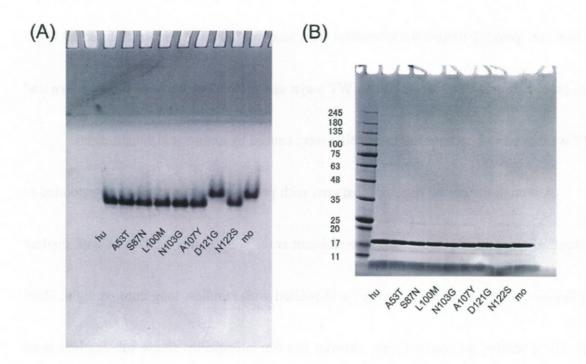


Fig. 6 Purified monomeric alpha-synuclein used in this study

(A) Native-PAGE and (B) SDS-PAGE data. Vertical numbers indicate molecular weight. The gels were stained with CBB.

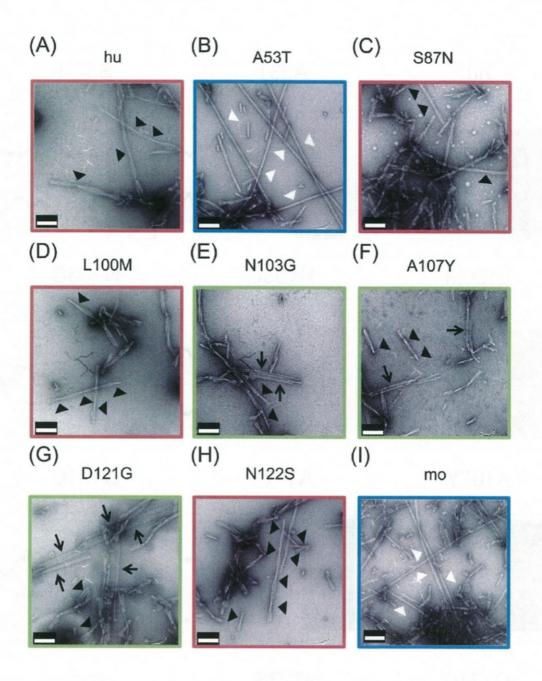


Fig. 7 Alpha-synuclein mutants with single substitution form distinct amyloid fibrils

Electron micrographs of (A) human WT a-syn, (I) mouse a-syn, and (B-H) other mutants a-syn. Scale bars show 100 nm. Black and white arrowheads indicate twisted sites and straight filaments, respectively. Black arrows indicate bundle type of filaments. Amyloid fibril morphologies of mutants were divided into 3 groups: Group A; twisted (red), Group B; straight (blue); Group C; twisted bundled fibrils (green).

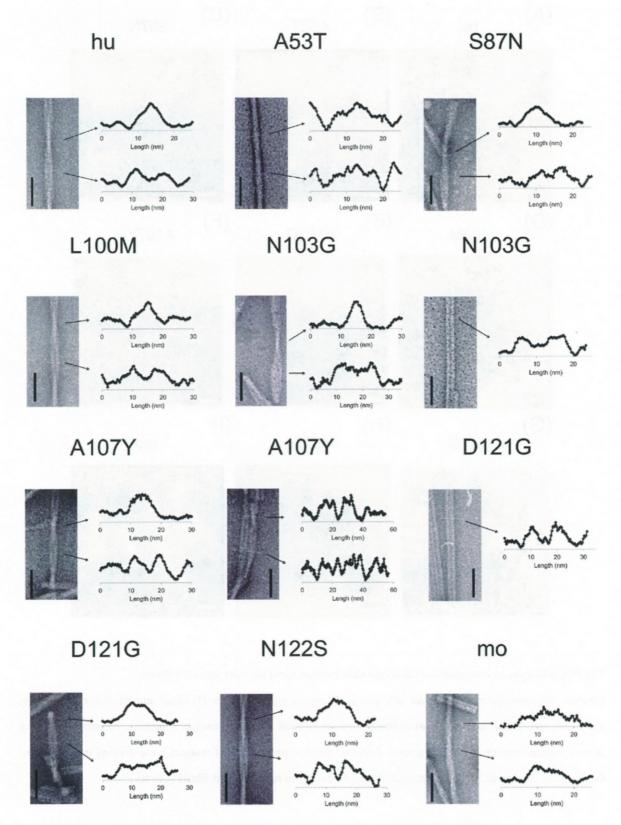
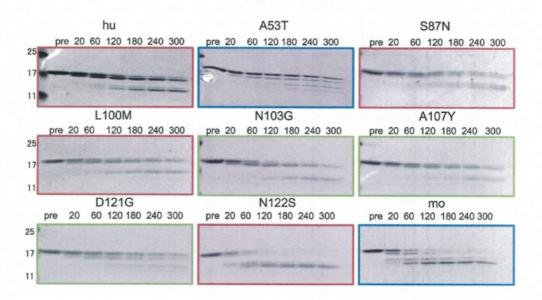


Fig. 8 Representative fibrils of human wild-type, mouse, and mutant alpha-synuclein

Representative fibrils are shown on the left side. Scale bars show 50 nm. Gray scales measured using ImageJ are shown on the right side. Low and high value indicate the black and white pixels in electron micrographs, respectively.

(A)



(B)

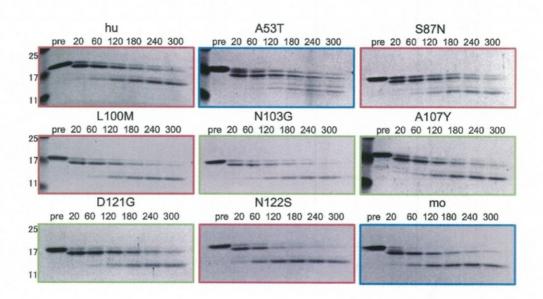


Fig. 9 Proteinase K and trypsin digestion experiments show distinct patterns in human wild-type, mouse, and mutants alpha-synuclein

Aggregates of human, mouse, and mutant alpha-synucleins were digested with (A) proteinase K and (B) trypsin. Samples were collected at each time point (20, 60, 120, 180, 240, and 300 s). Different digestion patterns were detected in SDS-PAGE gel stained with CBB.

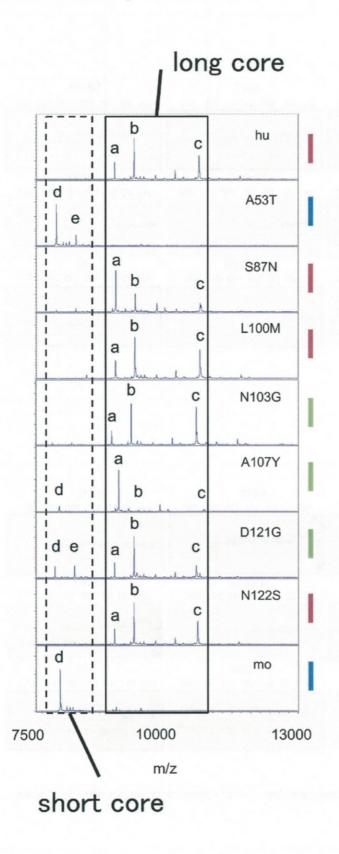


Fig. 10 Alpha-synuclein mutants with single substitution form distinct proteinase K-resistant core revealed by MALDI-TOF MS analysis

MALDI-TOF MS spectra (m/z 7500-13,000) of core peptides derived from human, mouse, and mutant a-syn aggregates are shown. Segments enclosed in rectangles with a solid and dashed lines are shown for long core (human-specific spectra area; a, b, c) and short core (mouse-specific spectra area; d, e), respectively. The classification of morphologies: Group A (red), Group B (blue), and Group C (green) are indicated in the right side.

3.3. Structural transmissibility of morphological and biochemical features by seeding

The results of the single substitutions experiments suggested that the primary sequence of a-syn is a strong structural determinant for fibrils generated by spontaneous aggregation. However, it is possible that other factors regulate this process. In this respect, we performed seeding experiments to investigate whether seeds could induce structures different from the spontaneously formed aggregates. We seeded human WT a-syn with the aggregates (PFF) of human, mouse or human point mutants (designated as hu-(seeds)). The predominant fibril morphologies of hu-(hu), hu-(S87N), hu-(L100M), and hu-(N122S) aggregates were of twisted-type as observed in the PFF seeds (Group A) (Fig. 11A, 11C, 11D, and 11H). In contrast, the predominant fibril morphology of hu-(A53T) and hu-(mo) were of straight-type as observed in those PFF seeds (Group B) (Fig. 11B and 11I). Furthermore, hu-(N103G), hu-(A107Y), and hu-(D121G) showed both twisted and bundles of two straight fibrils (Group C). Although the population was minor, we also observed twisted fibrils in all

the seed-induced aggregates even in hu-(mo) and hu-(A53T), possibly because of spontaneous aggregation of human WT a-syn. Representative fibrils are shown in Fig. 12. These results indicate that the morphological structure of the PFF seeds could be transmitted to the substrate (human WT a-syn), generating structures different from spontaneously formed aggregates of human WT a-syn.

Upon protease partial digestion, the digestion patterns of N122S and mouse a-syn fibrils showed different patterns from hu-(mo) and hu-(N122S) (Fig. 13A). However, other seed-induced aggregates showed band patterns nearly identical to those of the seeds. Thus, under these seeding conditions, human a-syn partly adopted the biochemical properties of the seeds as shown in trypsin digestion patterns (Fig. 13B). We further examined the amyloid fibril cores of seed-induced aggregates (Fig. 14). Group A and C (hu-(hu), hu-(S87N), hu-(L100M), hu-(N103G), hu-(A107Y), hu-(D121G), and hu-(N122S)) showed human-type long core peaks (a, b, and c). In contrast, protease-resistant core of Group B (hu-(A53T) and hu-(mo)) showed two peaks, which corresponded with that of the mouse-type short core. Because spontaneous aggregation of human WT a-syn could occur under our experimental condition, seed-induced aggregates in Group B also included a and b or c peak(s) in addition to d and e peaks. These results suggest that the protease resistant core of human a-syn seeded with mutant aggregates included the core of the spontaneous aggregates of human a-syn. However, the mass peak(s) of hu-(A107Y) core (m/z 10925.2, c*) did not correspond to those of human WT a-syn (m/z 10914.7, c) and A107Y aggregates core (m/z 9217.3, a). At this moment, it is hard to explain this different peak pattern observed between PFF seeds and seed-induced aggregate of A107Y. One possibility is that A107Y PFF seeds include multiple conformational species of minor species, whose conformations are different from the major structure of the seeds. Although minor differences were observed, the core patterns were highly consistent with those of the PFF seeds, strongly suggesting core structure transmission by seeding.

AGERA is often utilized to investigate protein complexation in greater detail (> 200 kDa) [71]. Thus, amyloid fibril states of each mutant PFF seeds and seed-induced aggregates were analyzed with AGERA. As shown in Fig. 15, human WT a-syn, S87N, and L100M (Group A) formed low intensities of high molecular weight SDS-stable aggregates (H), whereas N103G, A107Y, D121G, and mouse (Group B and Group C) showed higher intensities of high molecular weight SDS-stable aggregates. Although A53T and N122S showed ambiguous results of SDS-stable aggregates based on the morphological classification, thus, we considered that higher molecular weight complexes showed different

properties among mutants. We further examined the state of the SDS-stable aggregates by mutant seeding. Among the higher molecular weight SDS-stable aggregates (H), hu-(L100M), hu-(N103G), hu-(A107Y), and hu-(D121G) were quite similar to their seeds. On the other hand, hu-(hu), hu-(A53T), hu-(S87N), and hu-(mo) showed increased intensity than the seeds, suggesting that those mutant seeds accelerate the formation of higher molecular weight aggregates. These data implied that in some cases, these properties were transmitted to seed-induced aggregates and in the others, more high molecular weight complexes were formed than by the seeds, suggesting that PFF seeds accelerated aggregate formation.

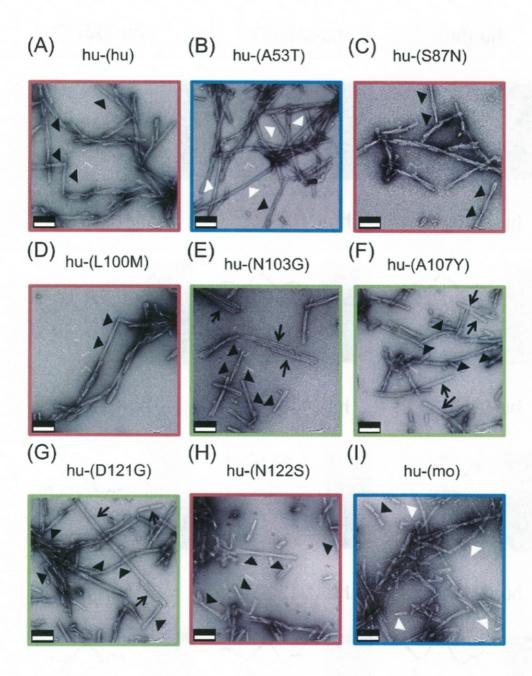


Fig. 11 Morphologies of mutation-dependent structures could be transmitted to human wild-type alpha-synuclein by seeding reactions.

(A–I) Electron micrographs of aggregates formed from human WT a-syn seeded with human, mouse or other mutant fibrils. Scale bars show 100 nm. Black and white arrowheads indicate twisted sites and straight filaments, respectively. Black arrows indicate bundle types of filaments. Amyloid fibril morphologies of human WT a-syn aggregates formed by seeding were divided into 3 groups: Group A; twisted (red), Group B; straight (blue); Group C; twisted fibrils with bundled (green).

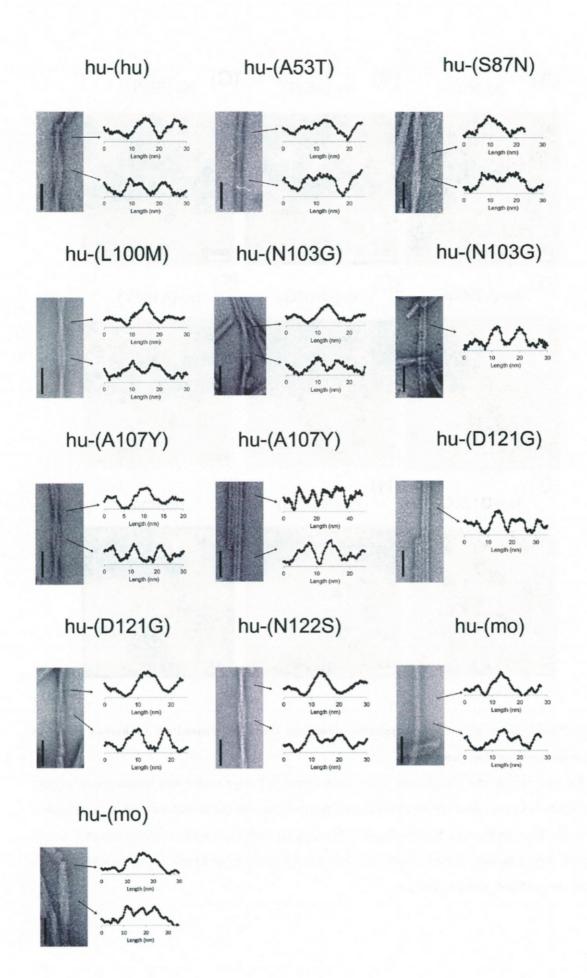
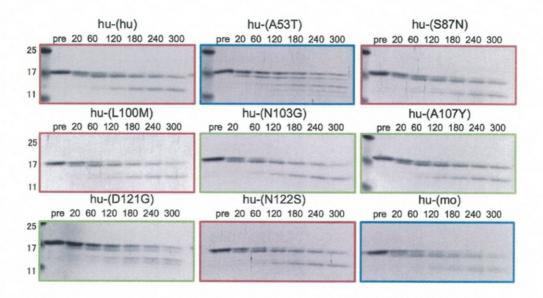


Fig. 12 Representative seed-induced fibrils of human wild-type alpha-synuclein

Representative fibrils are shown in left side. Scale bars show 50 nm. Gray scales measured using ImageJ are shown in right side. Low and high value mean black and white pixels in electron micrographs, respectively. Black arrows indicate the position measured in gray scales (white lines).

(A)



(B)

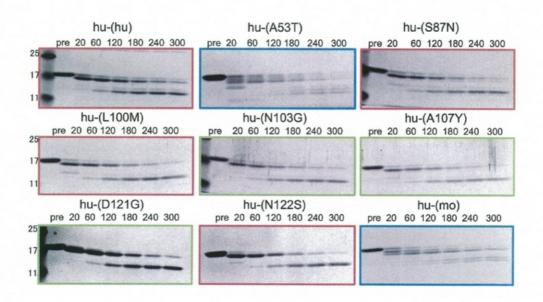


Fig. 13 Proteinase K and trypsin digestion experiments show distinct patterns in seed-induced aggregates Human, mouse, and mutant seed-induced alpha-synuclein aggregates were digested with (A) proteinase K and (B) trypsin. Samples were collected at each time point (20, 60, 120, 180, 240, and 300 s). Different digestion patterns were detected using SDS-PAGE gel stained with CBB.

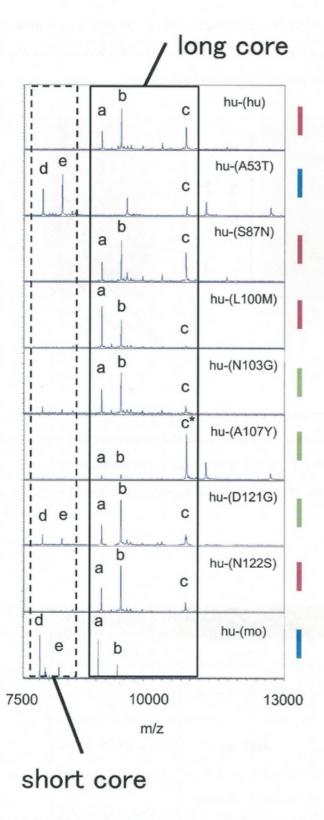


Fig. 14 Seed-induced aggregates show distinct proteinase K-resistant core corresponding to the pre-formed fibril seeds.

MALDI-TOF MS spectra (m/z 7500-13,000) of core peptides derived from seed induced aggregates of human WT a-syn with mutant PFF. Segments enclosed in rectangles with a solid and dashed lines are shown for long

core (human-specific spectra area; a, b, c, c*) and short core (mouse-specific spectra area; d, e), respectively. There is a minor difference in the spectra between c and c* in hu-(A107Y). The classification of morphologies: Group A (red), Group B (blue), and Group C (green) is indicated on the right side.

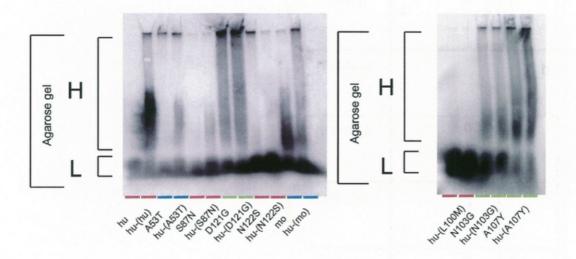


Fig. 15 AGERA reveals transmissibility of biochemical properties of aggregates

The aggregates without boiling were subjected to 1% agarose gel, followed by western blotting. The transferred membranes were stained with S1 antibody. (B) Solid lines indicate the positions of low molecular (L) and high molecular (H) area of SDS-stable a-syn aggregates. The classification of morphologies: Group A (red), Group B (blue), and Group C (green) are indicated.

Table 2. Summary of the results

	Group A	Group B	Group C
Morphology	twisted	straight	twisted with bundles
Protease-resistant core	long core	short core	long core
AGERA H	low	high	high
Mutant	hu, S87N, L100M, N122S	A53T, mo	N103G, A107Y, D121G
Seed-induced aggregate	hu-(hu), hu-(S87N), hu-(L100M), hu-(N122S)	hu-(A53T), hu-(mo)	hu-(N103G), hu-(A107Y), hu-(D121G)

Note: High molecular area of SDS-stable a-syn aggregates in AGERA is indicated by AGERA H. The intensities of AGERA H are described as low or high.

3.4. Biochemical and morphological classification of disease-associated mutant alpha-synuclein fibrils

To examine the relationship between the different disease phenotypes of synucleinopathies and the polymorphisms of aggregated a-syn proteins, we analyzed the aggregates derived from disease-associated a-syn mutations using biochemical techniques. Disease-associated a-syn mutations were located in the amphipathic N-terminal region (Fig. 16A). Purified monomeric states of a-syn were evaluated by native-PAGE and SDS-PAGE. the results of which indicated that familial missense mutations, associated with charged amino acids, altered the position of bands in native-PAGE (Fig. 16B and Fig. 17). We further carried out thermal denaturation of a-syn in presence of SYPRO Orange, which revealed that disease-associated mutations affected the thermal denaturation curve (Fig. 16C). Heat denaturation of all mutants, other than E46K, in presence of SYPRO Orange, resulted in a remarkable increase in fluorescence at around 50-60 °C. Together, these data suggest that the structurally diverse a-syn mutants exhibit distinct hydrophobic thermal stability in the monomeric states.

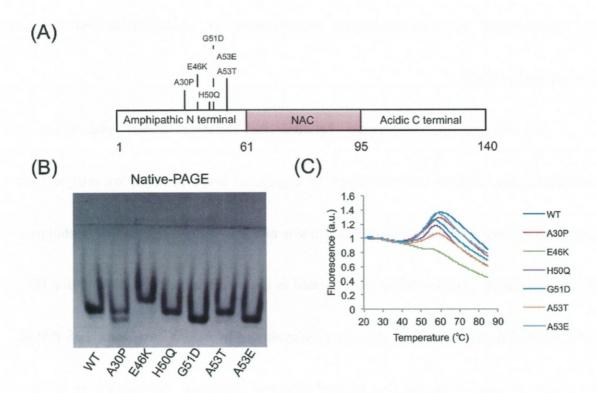


Fig. 16 Disease-associated monomeric mutants of alpha-synuclein form distinct states

(A) Schematic illustration of the structure of human a-syn (WT) with the three distinct domains (amphipathic N-terminal, NAC, and acidic C-terminal). Disease-associated mutations of a-syn are located in the amphipathic N-terminal regions (A30P, E46K, H50Q, G51D, A53T, and A53E). Amino acid residues are shown in the bottom. (B) Monomeric states of WT and disease-associated mutants were evaluated by native-PAGE stained with CBB. (C) Thermal denaturation was monitored by SYPRO Orange fluorescence in monomeric states of WT and disease-associated a-syn mutants. Data are means of 3 different wells.

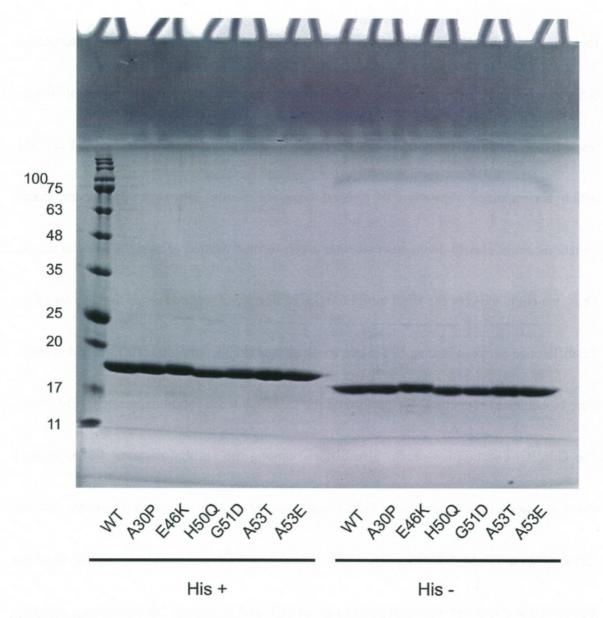


Fig. 17 Purified disease-associated monomeric mutants of alpha-synuclein

Monomeric states of disease-associated mutants of a-syn were detected in SDS-PAGE stained with CBB. Molecular weight is shown on the left. Presence and absence of His tags are indicated by His + or His -, respectively.

To examine the aggregated forms of disease-associated a-syn mutants, we observed the purified 7-day aggregated amyloid fibrils using EM (Fig. 18A). E46K formed predominantly twisted amyloid fibrils (arrowheads), whereas A30P, H50Q, G51D, and A53E

formed predominantly straight types, including bundled types. As in the interspecies difference, human WT a-syn and A53T formed twisted and straight types of fibrils, respectively. Bundled types of fibrils were also observed in N103G, A107Y, and D121G, which accompanied formation of twisted types of fibrils. However, disease-associated mutations could clearly distinguish whether a-syn formed twisted or straight types of fibrils. Thus, we could classify the fibril morphologies of disease-associated a-syn mutants based on the difference between human WT a-syn (twisted) and A53T (straight). To further determine their biochemical properties, we performed the GdnHCl denaturation experiment (Fig. 19A). The GdnHCl-denaturation curves also differed among the familial mutants. E46K showed lower resistance to denaturation by GdnHCl as detected in WT, compared with other mutants (denaturing at 1.5 M GdnHCl, Fig. 19B). When digested with proteinase K, the digested bands of a-syn mutants were similar to that of WT at 5 min (Fig. 20A), whereas different digested bands were obtained for disease-associated mutants at 120 min (Fig. 20B). Digested samples at 120 min were confirmed by MALDI-TOF MS analysis, indicating that proteinase K-resistant cores differed among the disease-associated a-syn mutants (Fig. 20C). The core of E46K and WT showed mainly longer spectra, (m/z 9552.9) and (m/z 9126.3 and m/z 9539.0), respectively, as compared with other disease-associated mutants. The main peak(s) of cores

in A30P (m/z 7330.6), G51D (m/z 7317.0 and m/z 7928.8), and A53T (m/z 7901.0) showed relatively shorter spectra than those of WT and E46K. On the other hand, the main peaks of cores in H50Q (m/z 7250.5, m/z 7682.3, m/z 10309.7, and m/z 10921.2) and A53E (m/z 7319.1, m/z 7390.5, m/z 10379.0, and m/z 10990.2) showed similar mass spectral pattern with short and long cores. Based on these results, we could classify the mutants according to the protease-resistant cores into three groups (WT and E46K; long, A30P, G51D, and A53T; short, and H50Q and A53E; short and long).

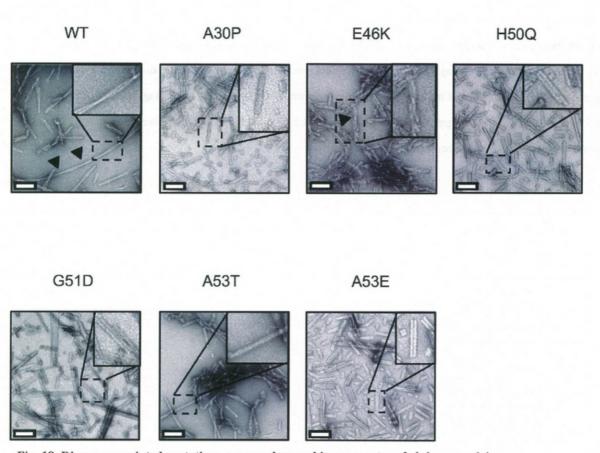


Fig. 18. Disease-associated mutations cause polymorphic aggregates of alpha-synuclein

Electron micrographs of WT and disease-associated a-syn mutant aggregates. Each segment enclosed in rectangle with a dashed line is zoomed in to show a representative amyloid fibril. The arrowheads indicate twisted type of amyloid fibrils. Scale bars indicate 100 nm.

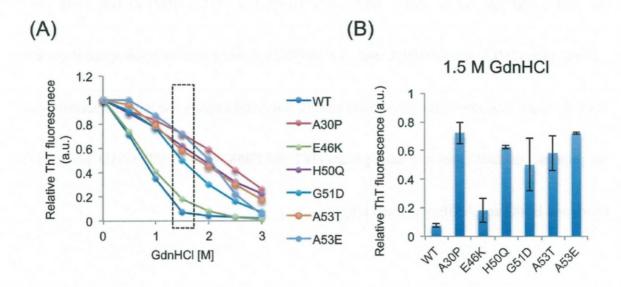


Fig. 19 Disease-associated mutations cause biochemical polymorphic aggregates of alpha-synuclein

(A) GdnHCl-denaturation assay indicates distinct biochemical properties of WT and disease-associated mutant aggregates. Segment enclosed in rectangle with dashed lines indicate the corresponding values of denaturation from 1.5 M GdnHCl, (B) Aggregation was quantified at 1.5 M GdnHCl in WT and disease-associated mutants. Means and standard errors of replicates (n = 3) are shown.

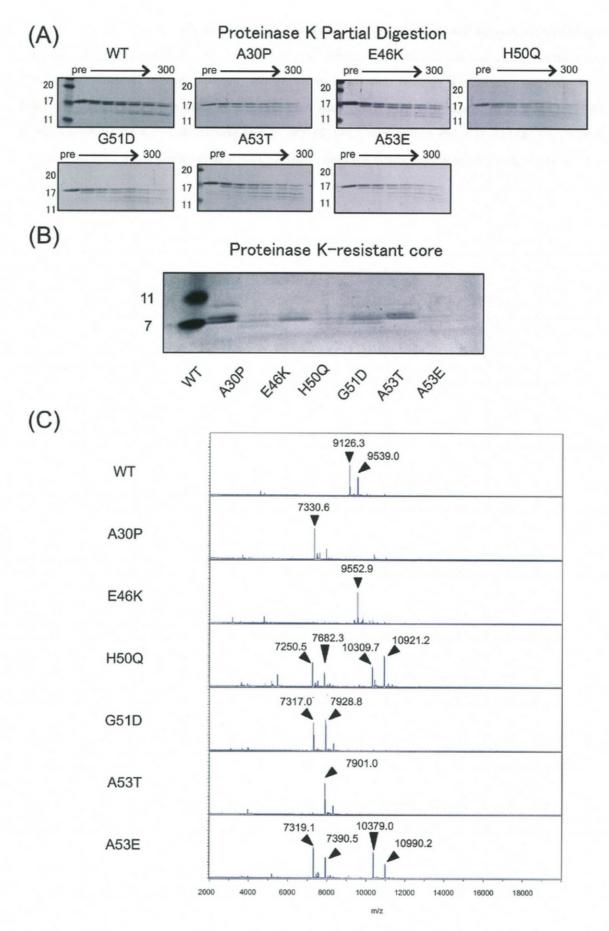


Fig. 20 Disease-associated mutations cause distinct proteinase K-resistant core

(A) Results of partial protease-digestion experiments using proteinase K. "Pre" indicates pre-digested samples; "300" indicates proteinase K reaction time (in seconds). Vertical numbers indicate molecular weight. (B) Different types of proteinase K-resistant core bands were detected by CBB staining in disease-associated mutants. (C) MALDI-TOF MS spectra (m/z 2,000–20,000) of core peptides derived from disease-associated mutants. The peaks for the protease-resistant fragment of disease-associated mutations and WT are indicated.

Chapter 4. Discussion

In this thesis, spontaneous aggregates of human and mouse a-syn showed distinct morphological and biochemical polymorphism based on the differences in their primary sequence. Additionally, a-syn monomers were able to adopt various structures upon aggregation with different PFF seeds (Table 3). Particularly, a single interspecies substitution, A53T, which is one of the familial PD mutations, was responsible for the mouse-type structures including straight morphology and short protease-resistant core, and could be transmitted to human a-syn by seeding. Furthermore, we clarified polymorphic aggregates derived from disease-associated mutations of a-syn, and successfully classified them to correspond with the types of synucleinopathies. The data presented here support the recent hypothesis that distinct polymorphic aggregates of a-syn might cause the distinct pathogenicity of synucleinopathies [36, 43, 72].

4.1. Human and mouse alpha-synuclein substitution

Recently, *in vivo* transmission experiment of human a-syn aggregate seeds into mouse was reported [48]. However, the precise difference of human and mouse a-syn has not been studied yet. It was reported that the N-terminal A53T substitution, which is known to cause early onset PD in humans and PD-like phenotype in transgenic mice [73], plays a

dominant role relative to the other substitutions in the NAC and C-terminal regions in speeding up the fibril assembly kinetics of mouse compared with human a-syn [52]. An NMR chemical shift analysis suggested that the growth process of fibrils is controlled by the nature of the secondary structure propensity in A53T region [52]. However, other biochemical properties between human and mouse a-syn fibrils had not been examined. Therefore, in this thesis, the human and mouse a-syn fibrils were first examined using biochemical and morphological methods. Biochemical analyses using proteases indicated that the two types of aggregates were distinct from each other. EM analysis showed that human and mouse a-syn formed predominantly two types of fibrils, twisted and straight. Based on the biochemical and morphological properties, the human a-syn fibrils could be clearly distinguished from those of the mouse a-syn. Through analysis of single substituted mutants of human a-syn, we the A53T was revealed to be responsible for the biochemical difference between human and mouse a-syn. The analyses presented here support the notion that the presence of A at position 53 may be an evolutionary adaptation to minimize PD in humans, as previously described [52].

4.2. Protease partial digestion and alpha-synuclein fibrils

It has been reported that possible conformational changes of a-syn PFFs at the N and C termini correlate with phenotypic conversion of different strain [38]. Therefore, we hypothesized that different conformation of a-syn fibrils detected by proteinase K partial digestion experiments could be due to difference in the two terminal region. As shown in Fig. 5 (A) and (B), human and mouse a-syn aggregates showed distinct patterns with protease partial digestion. Previously, proteinase K digestion of mouse PFFs showed a dramatically different pattern, indicating facile degradation at both N and C termini [51], which is consistent with our data. By using other proteases, such as trypsin, chymotrypsin, and pronase, they suggested that the differences in protease partial digestions between human and mouse a-syn PFFs were driven largely by the amino acid residues at position 53 and 87, although terminal regions of a-syn might also contribute to the overall structure of PFFs [51]. However, the current study failed to determine the responsible amino acids for the differences in partial digestion with proteases. The digestion pattern of A53T and S87N did not show patterns similar to that of mouse a-syn. This inconsistency between our study and previous study was probably due to the different strategy applied to determine the biochemical differences between human and mouse a-syn. We used single substitutions of a-syn targeting the seven divergent positions between mouse and human WT a-syn. In contrast, they used chimeric and truncated a-syn, in addition to two (A53T and S87N) single substitutions of a-syn [51]. Although our strategy provided insights into some differences between human and mouse a-syn experiments, future studies involving chimeric and truncated a-syn are required to examine the further differences, particularly in protease partial digestion experiments between human and mouse a-syn.

4.3. Protease-resistant core of alpha-synuclein fibrils

Amyloid structure has a common structure called core [74], which forms cross-beta sheets that are highly protease-resistant [66, 69, 70]. Solid-state NMR experiments showed a Greek-key motif in core regions of a-syn amyloid fibrils [25], which corresponds to the protease-resistant core determined by a previous study [75]. As for other amyloidogenic proteins, SOD1, tau, and prion proteins form fibrils with a distinct protease-resistant core that partly corresponds with morphological or physiological differences [66, 69, 70, 75].

According to a previous study [75], the proteinase K-resistant filament cores of recombinant a-syn are ~7–9 kDa fragments truncated at N and C terminal region. The study analyzed the amino-terminal sequences of the three major bands migrating at 7, 8, and 9-kDa

detected in proteinase K-treated a-syn filaments directly by a protein sequencer. The 7- and 8-kDa proteinase K-resistant fragments consisted of polypeptides starting at the same N terminus (i.e. residue 31 of a-syn) but ending at a different C-terminal position. The 9-kDa band gave two sequences, which corresponded to the amino acid terminus from the residues 19- and 20- of a-syn, respectively. The structure of the minimal fragment that constitutes the protease-resistant core of a-syn is residues 31-109, which corresponded with the 7-kDa proteinase K-resistant fragment. In our experiments, we could detect proteinase-K resistant core in human a-syn aggregates (the long cores). The spectrum at m/z 9127.1 might correspond to the 9-kDa fragment in the previous study. In contrast, the protease-resistant core (m/z 7978.6) detected in mouse a-syn aggregates corresponded to the 7-kDa fragment, which was the minimal fragment (the short cores). Thus, our data implied that mouse a-syn fibrils easily form minimal fragment of proteinase-K resistant core than the human WT a-syn. Based on the N-terminal sequences of the core determined by a previous study, these two types of core differed at N-terminal sequences (short: 31- or long: 19 or 20-). Together, these data suggest that the structures of the two types of fibrils are different at N-terminal region.

Interestingly, our mutagenesis approach revealed that A53T mutant, the only interspecies substitution located in the N-terminal region, formed the short core, which

and mouse-type core structures could be transmitted to human WT a-syn. These data implied that human WT a-syn has the intrinsic potential to form two different proteinase-K resistant cores, either of which is eventually selected depending on amino acid sequences and/or the presence of PFF seeds.

4.4. Amyloid fibril polymorphisms of human and mouse alpha-synuclein based on the morphologies

Morphologically, we identified twisted and straight types of fibrils in human and mouse a-syn, respectively. It was reported that in contrast to the human a-syn fibril structure, the mouse a-syn fibrils consist of two or even more protofilaments, with residues of G84–V95 constituting the possible protofilament-protofilament interface [53]. A recent cryo-EM study demonstrated that human a-syn protofilaments comprise of two different regions, namely, NAC (residues 68-78) or pre-NAC (residues 46-56) regions, generating polymorphic a-syn fibrils with rod or twister structure, respectively [43]. The identified human and mouse a-syn fibrils in this study resembled the twister and rod morphologies, respectively, implying

that these fibrils differed in their protofilament-protofilament interface.

Additionally, we determined that twisted and straight types of fibrils are composed of the long and short proteinase K-resistant cores, respectively. Given that the distinctive morphologies are caused by different regions of protofilament packing, our data imply that the length of proteinase K-resistant cores are related with the protofilament packing regions. Future studies are required to analyze to clarify the direct relationship between the morphologies and proteinase K-resistant cores, perhaps by using cryo-EM.

4.5. Disease-associated alpha-synuclein mutations

Based on the data obtained on the polymorphic amyloid fibrils in human and mouse a-syn, the states of monomeric and fibrillar a-syn were examined to understand the relationship between the properties of fibrils and the diversity of synucleinopathies. Mutations in *SNCA* gene account for < 1 % of PD in the general population; however, the aggregated forms of *SNCA*-encoded protein, a-syn was commonly present in patients with sporadic PD [76]. Six disease-associated a-syn mutations have been implicated in PD as well as other synucleinopathies. The codon 51 and 53 mutations in the *SNCA* gene (G51D, A53T, and A53E) cause MSA-like phenotype, while the codon 46 mutation (E46K) causes a DLB

phenotype [55, 57, 77, 78]. Recently, the importance of disease-associated a-syn mutants was reconfirmed, since they resulted in polymorphic aggregates under *in vitro* conditions [78-82]. However, as of now, no biochemical method could classify the mutants based on the types of synucleinopathy, including PD, DLB, and MSA. Therefore, they were classified using *in vitro* experiments by performing morphological and biochemical comparisons of structures between human and mouse a-syn.

The disease-associated mutants may be classified into PD (A30P and H50Q), PD and MSA (A53T, G51D, and A53E), and PD and DLB (E46K) based on clinical and pathological phenotypes (Table 3) [55]. In this thesis, the biochemical and morphological properties of these mutants were differentiated. Mutants associated with PD or PD with MSA formed straight amyloid fibrils, which were more resistant to denaturation by GdnHCl. PD or PD with MSA showed short core or short and long core demonstrated by the proteinase K-resistant core experiments. In contrast, in DLB type, E46K mutant formed twisted amyloid fibrils, with low resistance to denaturation by GdnHCl, similar to WT, which showed the long core. Using electron microscopy, GdnHCl denaturation assay, and protease-resistant experiments, we successfully classified the disease-associated mutants based on their biochemical and morphological properties of fibrils generated under *in vitro* condition.

Using EM, it was observed that A30P forms straight fibrils while E46K forms twisted fibrils, which correspond with a previous study [79]. In another report, H50Q had been shown to have higher resistance to GdnHCl-denaturation compared with WT [83], which is consistent with our results. However, in this study, G51D and A53T also formed straight amyloid fibrils, which was inconsistent with previous results [80, 81]; these differences may be attributed to the use of TAT mutants to avert mis-incorporation of cysteine mutation or different conditions used to generate the fibrils in our *in vitro* experiments [63].

The classification of polymorphic a-syn aggregates using proteinase K-digestion has been mainly performed using partial digestion [36, 38, 42]. However, we could not detect any significant difference among the disease-associated mutants in partial digestion experiments with short incubation times (5 min) (Fig. 20A). Instead, we could demonstrate the differences between proteinase K-resistant cores among the disease-associated mutants at longer incubation time (120 min) (Fig. 20B and 20C). E46K mutant showed unique proteinase K-resistant core (long core) in mass spectrum compared with other disease-associated mutants (short core or short and long core). The *in vitro* results of proteinase K digestion-resistant cores could partly correlate to the different pathologies associated with

differently structured a-syn, and implicate the possibility of classification of synucleinopathies, as performed in tauopathy [69, 84]. The exact amino acid sequence of proteinase K-resistant core of the aggregated forms of disease-associated a-syn mutants should be clarified to reveal the precise pathological mechanism of synucleinopathies.

Table 3. Summary of comparisons of human wild-type and disease-associated alpha-synuclein mutants

a-syn variant	Clinical Phenotype	Morphology of amyloid fibrils	Resistance to GdnHCl	Protease-resista nt core
WT		twisted	low	long
A30P	Classic PD	straight	high	short
E46K	DLB	twisted	low	long
H50Q	Classic PD	straight	high	short and long
G51D	PD with MSA	straight	high	short
A53T	PD with MSA	straight	high	short
A53E	PD with MSA	straight	high	short and long

Note. Classic PD (A30P and H50Q), PD with MSA (G51D, A53T, and A53E), and DLB (E46K) synucleinopathies were classified based on disease-associated mutations. The classification of clinical

phenotypes in various synucleinopathies are described according to a previous review article [55].

4.6. Concluding remarks

Based on the results presented here, the distinct morphological observations of fibrils in a-syn were highly related with the protease-resistant core detected with mass spectrometry. Against expectations, the protease-partial digestion experiment did not correspond to the morphological differences, which implied that fuzzy coat regions of a-syn fibrils might not significantly contribute to the distinct morphological observations. Together with previous reports, the current findings indicate that the identified morphologically distinct fibrils (twisted and straight in human and mouse a-syn, respectively) are related with the molecular structural difference in the protofilament-protofilament interface.

Additionally, a single substitution of A53T was identified to be responsible for the differences between human and mouse a-syn. The disease-associated mutant analyses further imply that the morphological distinctiveness of mutant a-syn fibrils can be classified as either twisted (WT and E46K) or straight (A30P, H50Q, G51D, A53T, and A53E). Moreover, protease digestion experiments revealed that the morphological classification could correspond to the length of protease-resistant cores and the resistance from GdnHCl denaturation, although the disease-associated mutations did not affect the partial digestion

patterns. These results suggest that the protease-resistant cores are altered by changes in molecular structural conformations, which are related with the morphologically distinctiveness of fibrillar states of a-syn, and may contribute to the pathological distinctiveness of synucleinopathies.

Importantly, transmission of the structural properties of straight fibrils could be achieved upon seeding with human a-syn; this phenomenon was more prominent for A53T fibrils. We speculate that the A53T mutation may alter properties of the interphase for protofilament interactions, leading to alteration of fibrillar morphology, causing severe pathogenicity *in vivo* compared with human WT a-syn fibrils. This thesis has a major limitation: the biological functions and pathogenicity of the fibrils could not be investigated. In the future, further studies using cell or animal models need to be performed to deepen our understanding of a-syn structural polymorphism and investigate the potential mechanism by which it mediates the distinct pathogenicity of synucleinopathies.

Chapter 5 References

- [1] J.E. Galvin, V.M. Lee, J.Q. Trojanowski, Synucleinopathies: clinical and pathological implications, Arch Neurol, 58 (2001) 186-190.
- [2] K.A. Jellinger, Neuropathological spectrum of synucleinopathies, Mov Disord, 18 Suppl 6 (2003) S2-12.
- [3] M.G. Spillantini, R.A. Crowther, R. Jakes, M. Hasegawa, M. Goedert, alpha-Synuclein in filamentous inclusions of Lewy bodies from Parkinson's disease and dementia with lewy bodies, Proc Natl Acad Sci U S A, 95 (1998) 6469-6473.
- [4] K. Wakabayashi, M. Yoshimoto, S. Tsuji, H. Takahashi, Alpha-synuclein immunoreactivity in glial cytoplasmic inclusions in multiple system atrophy, Neurosci Lett, 249 (1998) 180-182.
- [5] M.G. Spillantini, M. Goedert, The alpha-synucleinopathies: Parkinson's disease, dementia with Lewy bodies, and multiple system atrophy, Ann N Y Acad Sci, 920 (2000) 16-27.
- [6] K.A. Conway, J.D. Harper, P.T. Lansbury, Jr., Fibrils formed in vitro from alpha-synuclein and two mutant forms linked to Parkinson's disease are typical amyloid, Biochemistry, 39 (2000) 2552-2563.
- [7] M. Hashimoto, L.J. Hsu, A. Sisk, Y. Xia, A. Takeda, M. Sundsmo, E. Masliah, Human recombinant NACP/alpha-synuclein is aggregated and fibrillated in vitro: relevance for Lewy body disease, Brain Res, 799 (1998) 301-306.
- [8] M.R. Ma, Z.W. Hu, Y.F. Zhao, Y.X. Chen, Y.M. Li, Phosphorylation induces distinct alpha-synuclein strain formation, Sci Rep, 6 (2016) 37130.
- [9] A. Shimozawa, M. Ono, D. Takahara, A. Tarutani, S. Imura, M. Masuda-Suzukake, M. Higuchi, K. Yanai, S.I. Hisanaga, M. Hasegawa, Propagation of pathological alpha-synuclein in marmoset brain, Acta Neuropathol Commun, 5 (2017) 12.
- [10] K.C. Luk, V. Kehm, J. Carroll, B. Zhang, P. O'Brien, J.Q. Trojanowski, V.M. Lee, Pathological alpha-synuclein transmission initiates Parkinson-like neurodegeneration in nontransgenic mice, Science, 338 (2012) 949-953.
- [11] M.E. Bernis, J.T. Babila, S. Breid, K.A. Wusten, U. Wullner, G. Tamguney, Prion-like propagation of human brain-derived alpha-synuclein in transgenic mice expressing human wild-type alpha-synuclein, Acta Neuropathol Commun, 3 (2015) 75.
- [12] S.B. Prusiner, A.L. Woerman, D.A. Mordes, J.C. Watts, R. Rampersaud, D.B. Berry, S. Patel, A. Oehler, J.K. Lowe, S.N. Kravitz, D.H. Geschwind, D.V. Glidden, G.M. Halliday, L.T. Middleton, S.M. Gentleman, L.T. Grinberg, K. Giles, Evidence for alpha-synuclein prions causing multiple system atrophy in humans with parkinsonism, Proc Natl Acad Sci U

- S A, 112 (2015) E5308-5317.
- [13] I.J. Siddiqui, N. Pervaiz, A.A. Abbasi, The Parkinson Disease gene SNCA: Evolutionary and structural insights with pathological implication, Sci Rep, 6 (2016) 24475.
- [14] V.N. Uversky, J. Li, P. Souillac, I.S. Millett, S. Doniach, R. Jakes, M. Goedert, A.L. Fink, Biophysical properties of the synucleins and their propensities to fibrillate: inhibition of alpha-synuclein assembly by beta- and gamma-synucleins, J Biol Chem, 277 (2002) 11970-11978.
- [15] H. Snyder, K. Mensah, C. Hsu, M. Hashimoto, I.G. Surgucheva, B. Festoff, A. Surguchov, E. Masliah, A. Matouschek, B. Wolozin, beta-Synuclein reduces proteasomal inhibition by alpha-synuclein but not gamma-synuclein, J Biol Chem, 280 (2005) 7562-7569.
- [16] M.G. Spillantini, M.L. Schmidt, V.M. Lee, J.Q. Trojanowski, R. Jakes, M. Goedert, Alpha-synuclein in Lewy bodies, Nature, 388 (1997) 839-840.
- [17] K. Nishioka, C. Wider, C. Vilarino-Guell, A.I. Soto-Ortolaza, S.J. Lincoln, J.M. Kachergus, B. Jasinska-Myga, O.A. Ross, A. Rajput, C.A. Robinson, T.J. Ferman, Z.K. Wszolek, D.W. Dickson, M.J. Farrer, Association of alpha-, beta-, and gamma-Synuclein with diffuse lewy body disease, Arch Neurol, 67 (2010) 970-975.
- [18] P. Oeckl, F. Metzger, M. Nagl, C.A. von Arnim, S. Halbgebauer, P. Steinacker, A.C. Ludolph, M. Otto, Alpha-, Beta-, and Gamma-synuclein Quantification in Cerebrospinal Fluid by Multiple Reaction Monitoring Reveals Increased Concentrations in Alzheimer's and Creutzfeldt-Jakob Disease but No Alteration in Synucleinopathies, Mol Cell Proteomics, 15 (2016) 3126-3138.
- [19] M. Fujita, S. Sugama, K. Sekiyama, A. Sekigawa, T. Tsukui, M. Nakai, M. Waragai, T. Takenouchi, Y. Takamatsu, J. Wei, E. Rockenstein, A.R. Laspada, E. Masliah, S. Inoue, M. Hashimoto, A beta-synuclein mutation linked to dementia produces neurodegeneration when expressed in mouse brain, Nat Commun, 1 (2010) 110.
- [20] N. Ninkina, O. Peters, S. Millership, H. Salem, H. van der Putten, V.L. Buchman, Gamma-synucleinopathy: neurodegeneration associated with overexpression of the mouse protein, Hum Mol Genet, 18 (2009) 1779-1794.
- [21] A.L. Fink, The aggregation and fibrillation of alpha-synuclein, Acc Chem Res, 39 (2006) 628-634.
- [22] L. Giehm, D.I. Svergun, D.E. Otzen, B. Vestergaard, Low-resolution structure of a vesicle disrupting & alpha;-synuclein oligomer that accumulates during fibrillation, Proc Natl Acad Sci U S A, 108 (2011) 3246-3251.
- [23] A.K. Buell, C. Galvagnion, R. Gaspar, E. Sparr, M. Vendruscolo, T.P. Knowles, S. Linse, C.M. Dobson, Solution conditions determine the relative importance of nucleation and

- growth processes in alpha-synuclein aggregation, Proc Natl Acad Sci U S A, 111 (2014) 7671-7676.
- [24] D. Pinotsi, C.H. Michel, A.K. Buell, R.F. Laine, P. Mahou, C.M. Dobson, C.F. Kaminski, G.S. Kaminski Schierle, Nanoscopic insights into seeding mechanisms and toxicity of alpha-synuclein species in neurons, Proc Natl Acad Sci U S A, 113 (2016) 3815-3819.
- [25] M.D. Tuttle, G. Comellas, A.J. Nieuwkoop, D.J. Covell, D.A. Berthold, K.D. Kloepper, J.M. Courtney, J.K. Kim, A.M. Barclay, A. Kendall, W. Wan, G. Stubbs, C.D. Schwieters, V.M. Lee, J.M. George, C.M. Rienstra, Solid-state NMR structure of a pathogenic fibril of full-length human alpha-synuclein, Nat Struct Mol Biol, 23 (2016) 409-415.
- [26] R.A. Crowther, S.E. Daniel, M. Goedert, Characterisation of isolated alpha-synuclein filaments from substantia nigra of Parkinson's disease brain, Neurosci Lett, 292 (2000) 128-130.
- [27] O.S. Makin, E. Atkins, P. Sikorski, J. Johansson, L.C. Serpell, Molecular basis for amyloid fibril formation and stability, Proc Natl Acad Sci U S A, 102 (2005) 315-320.
- [28] C.M. Wischik, M. Novak, H.C. Thogersen, P.C. Edwards, M.J. Runswick, R. Jakes, J.E. Walker, C. Milstein, M. Roth, A. Klug, Isolation of a fragment of tau derived from the core of the paired helical filament of Alzheimer disease, Proc Natl Acad Sci U S A, 85 (1988) 4506-4510.
- [29] D.M. Fowler, A.V. Koulov, W.E. Balch, J.W. Kelly, Functional amyloid--from bacteria to humans, Trends Biochem Sci, 32 (2007) 217-224.
- [30] E.G. Hutchinson, J.M. Thornton, The Greek key motif: extraction, classification and analysis, Protein Eng, 6 (1993) 233-245.
- [31] R. Guerrero-Ferreira, N.M. Taylor, D. Mona, P. Ringler, M.E. Lauer, R. Riek, M. Britschgi, H. Stahlberg, Cryo-EM structure of alpha-synuclein fibrils, Elife, 7 (2018).
- [32] D.F. Lazaro, E.F. Rodrigues, R. Langohr, H. Shahpasandzadeh, T. Ribeiro, P. Guerreiro, E. Gerhardt, K. Krohnert, J. Klucken, M.D. Pereira, B. Popova, N. Kruse, B. Mollenhauer, S.O. Rizzoli, G.H. Braus, K.M. Danzer, T.F. Outeiro, Systematic comparison of the effects of alpha-synuclein mutations on its oligomerization and aggregation, PLoS Genet, 10 (2014) e1004741.
- [33] J.C. Watts, K. Giles, A. Oehler, L. Middleton, D.T. Dexter, S.M. Gentleman, S.J. DeArmond, S.B. Prusiner, Transmission of multiple system atrophy prions to transgenic mice, Proc Natl Acad Sci U S A, 110 (2013) 19555-19560.
- [34] A.L. Woerman, J. Stohr, A. Aoyagi, R. Rampersaud, Z. Krejciova, J.C. Watts, T. Ohyama, S. Patel, K. Widjaja, A. Oehler, D.W. Sanders, M.I. Diamond, W.W. Seeley, L.T.

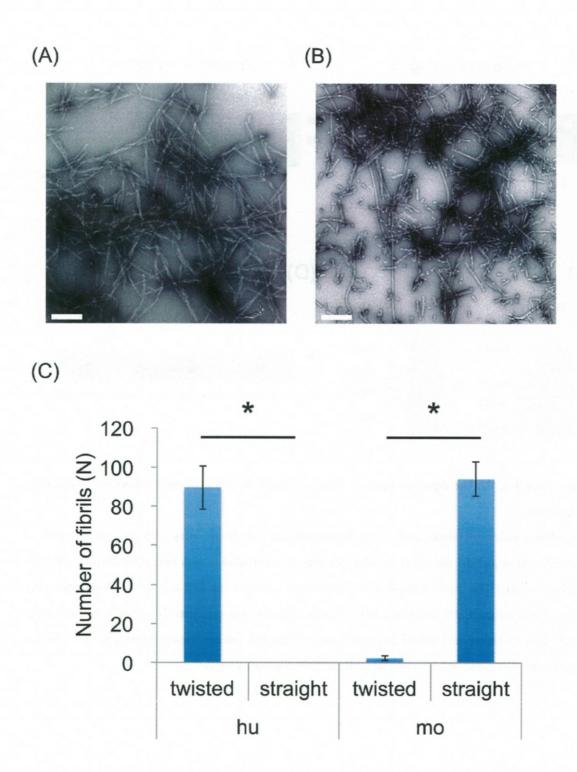
- Middleton, S.M. Gentleman, D.A. Mordes, T.C. Sudhof, K. Giles, S.B. Prusiner, Propagation of prions causing synucleinopathies in cultured cells, Proc Natl Acad Sci U S A, 112 (2015) E4949-4958.
- [35] A.L. Woerman, S.A. Kazmi, S. Patel, Y. Freyman, A. Oehler, A. Aoyagi, D.A. Mordes, G.M. Halliday, L.T. Middleton, S.M. Gentleman, S.H. Olson, S.B. Prusiner, MSA prions exhibit remarkable stability and resistance to inactivation, Acta Neuropathol, 135 (2018) 49-63.
- [36] C. Peng, R.J. Gathagan, D.J. Covell, C. Medellin, A. Stieber, J.L. Robinson, B. Zhang, R.M. Pitkin, M.F. Olufemi, K.C. Luk, J.Q. Trojanowski, V.M. Lee, Cellular milieu imparts distinct pathological alpha-synuclein strains in alpha-synucleinopathies, Nature, 557 (2018) 558-563.
- [37] W. Peelaerts, L. Bousset, A. Van der Perren, A. Moskalyuk, R. Pulizzi, M. Giugliano, C. Van den Haute, R. Melki, V. Baekelandt, alpha-Synuclein strains cause distinct synucleinopathies after local and systemic administration, Nature, 522 (2015) 340-344.
- [38] J.L. Guo, D.J. Covell, J.P. Daniels, M. Iba, A. Stieber, B. Zhang, D.M. Riddle, L.K. Kwong, Y. Xu, J.Q. Trojanowski, V.M. Lee, Distinct alpha-synuclein strains differentially promote tau inclusions in neurons, Cell, 154 (2013) 103-117.
- [39] C. Kim, G. Lv, J.S. Lee, B.C. Jung, M. Masuda-Suzukake, C.S. Hong, E. Valera, H.J. Lee, S.R. Paik, M. Hasegawa, E. Masliah, D. Eliezer, S.J. Lee, Exposure to bacterial endotoxin generates a distinct strain of alpha-synuclein fibril, Sci Rep, 6 (2016) 30891.
- [40] L. Bousset, L. Pieri, G. Ruiz-Arlandis, J. Gath, P.H. Jensen, B. Habenstein, K. Madiona, V. Olieric, A. Bockmann, B.H. Meier, R. Melki, Structural and functional characterization of two alpha-synuclein strains, Nat Commun, 4 (2013) 2575.
- [41] H. Kumar, J. Singh, P. Kumari, J.B. Udgaonkar, Modulation of the extent of structural heterogeneity in alpha-synuclein fibrils by the small molecule thioflavin T, J Biol Chem, 292 (2017) 16891-16903.
- [42] A. Villar-Pique, T. Lopes da Fonseca, R. Sant'Anna, E.M. Szego, L. Fonseca-Ornelas, R. Pinho, A. Carija, E. Gerhardt, C. Masaracchia, E. Abad Gonzalez, G. Rossetti, P. Carloni, C.O. Fernandez, D. Foguel, I. Milosevic, M. Zweckstetter, S. Ventura, T.F. Outeiro, Environmental and genetic factors support the dissociation between alpha-synuclein aggregation and toxicity, Proc Natl Acad Sci U S A, 113 (2016) E6506-E6515.
- [43] B. Li, P. Ge, K.A. Murray, P. Sheth, M. Zhang, G. Nair, M.R. Sawaya, W.S. Shin, D.R. Boyer, S. Ye, D.S. Eisenberg, Z.H. Zhou, L. Jiang, Cryo-EM of full-length alpha-synuclein reveals fibril polymorphs with a common structural kernel, Nat Commun, 9 (2018) 3609.
- [44] A. Iyer, S.J. Roeters, V. Kogan, S. Woutersen, M. Claessens, V. Subramaniam,

- C-Terminal Truncated alpha-Synuclein Fibrils Contain Strongly Twisted beta-Sheets, J Am Chem Soc, 139 (2017) 15392-15400.
- [45] P. Chien, J.S. Weissman, Conformational diversity in a yeast prion dictates its seeding specificity, Nature, 410 (2001) 223-227.
- [46] R.A. Moore, I. Vorberg, S.A. Priola, Species barriers in prion diseases--brief review, Arch Virol Suppl, (2005) 187-202.
- [47] D.A. Kocisko, S.A. Priola, G.J. Raymond, B. Chesebro, P.T. Lansbury, Jr., B. Caughey, Species specificity in the cell-free conversion of prion protein to protease-resistant forms: a model for the scrapie species barrier, Proc Natl Acad Sci U S A, 92 (1995) 3923-3927.
- [48] M.B. Fares, B. Maco, A. Oueslati, E. Rockenstein, N. Ninkina, V.L. Buchman, E. Masliah, H.A. Lashuel, Induction of de novo alpha-synuclein fibrillization in a neuronal model for Parkinson's disease, Proc Natl Acad Sci U S A, 113 (2016) E912-921.
- [49] M. Masuda-Suzukake, T. Nonaka, M. Hosokawa, T. Oikawa, T. Arai, H. Akiyama, D.M. Mann, M. Hasegawa, Prion-like spreading of pathological alpha-synuclein in brain, Brain, 136 (2013) 1128-1138.
- [50] A. Okuzumi, M. Kurosawa, T. Hatano, M. Takanashi, S. Nojiri, T. Fukuhara, T. Yamanaka, H. Miyazaki, S. Yoshinaga, Y. Furukawa, T. Shimogori, N. Hattori, N. Nukina, Rapid dissemination of alpha-synuclein seeds through neural circuits in an in-vivo prion-like seeding experiment, Acta Neuropathol Commun, 6 (2018) 96.
- [51] K.C. Luk, D.J. Covell, V.M. Kehm, B. Zhang, I.Y. Song, M.D. Byrne, R.M. Pitkin, S.C. Decker, J.Q. Trojanowski, V.M. Lee, Molecular and Biological Compatibility with Host Alpha-Synuclein Influences Fibril Pathogenicity, Cell Rep, 16 (2016) 3373-3387.
- [52] L. Kang, K.P. Wu, M. Vendruscolo, J. Baum, The A53T mutation is key in defining the differences in the aggregation kinetics of human and mouse alpha-synuclein, J Am Chem Soc, 133 (2011) 13465-13470.
- [53] G. Lv, A. Kumar, Y. Huang, D. Eliezer, A Protofilament-Protofilament Interface in the Structure of Mouse alpha-Synuclein Fibrils, Biophys J, 114 (2018) 2811-2819.
- [54] S. Hwang, P. Fricke, M. Zinke, K. Giller, J.S. Wall, D. Riedel, S. Becker, A. Lange, Comparison of the 3D structures of mouse and human alpha-synuclein fibrils by solid-state NMR and STEM, J Struct Biol, (2018).
- [55] H.T. Whittaker, Y. Qui, C. Bettencourt, H. Houlden, Multiple system atrophy: genetic risks and alpha-synuclein mutations, F1000Res, 6 (2017) 2072.
- [56] M.H. Polymeropoulos, C. Lavedan, E. Leroy, S.E. Ide, A. Dehejia, A. Dutra, B. Pike, H. Root, J. Rubenstein, R. Boyer, E.S. Stenroos, S. Chandrasekharappa, A. Athanassiadou, T. Papapetropoulos, W.G. Johnson, A.M. Lazzarini, R.C. Duvoisin, G. Di Iorio, L.I. Golbe, R.L.

- Nussbaum, Mutation in the alpha-synuclein gene identified in families with Parkinson's disease, Science, 276 (1997) 2045-2047.
- [57] J.J. Zarranz, J. Alegre, J.C. Gomez-Esteban, E. Lezcano, R. Ros, I. Ampuero, L. Vidal, J. Hoenicka, O. Rodriguez, B. Atares, V. Llorens, E. Gomez Tortosa, T. del Ser, D.G. Munoz, J.G. de Yebenes, The new mutation, E46K, of alpha-synuclein causes Parkinson and Lewy body dementia, Ann Neurol, 55 (2004) 164-173.
- [58] S. Lesage, M. Anheim, F. Letournel, L. Bousset, A. Honore, N. Rozas, L. Pieri, K. Madiona, A. Durr, R. Melki, C. Verny, A. Brice, G. French Parkinson's Disease Genetics Study, G51D alpha-synuclein mutation causes a novel parkinsonian-pyramidal syndrome, Ann Neurol, 73 (2013) 459-471.
- [59] P. Pasanen, L. Myllykangas, M. Siitonen, A. Raunio, S. Kaakkola, J. Lyytinen, P.J. Tienari, M. Poyhonen, A. Paetau, Novel alpha-synuclein mutation A53E associated with atypical multiple system atrophy and Parkinson's disease-type pathology, Neurobiol Aging, 35 (2014) 2180 e2181-2185.
- [60] V.N. Uversky, Looking at the recent advances in understanding alpha-synuclein and its aggregation through the proteoform prism, F1000Res, 6 (2017) 525.
- [61] L.R. Lemkau, G. Comellas, S.W. Lee, L.K. Rikardsen, W.S. Woods, J.M. George, C.M. Rienstra, Site-specific perturbations of alpha-synuclein fibril structure by the Parkinson's disease associated mutations A53T and E46K, PLoS One, 8 (2013) e49750.
- [62] S. Appel-Cresswell, C. Vilarino-Guell, M. Encarnacion, H. Sherman, I. Yu, B. Shah, D. Weir, C. Thompson, C. Szu-Tu, J. Trinh, J.O. Aasly, A. Rajput, A.H. Rajput, A. Jon Stoessl, M.J. Farrer, Alpha-synuclein p.H50Q, a novel pathogenic mutation for Parkinson's disease, Mov Disord, 28 (2013) 811-813.
- [63] M. Masuda, N. Dohmae, T. Nonaka, T. Oikawa, S. Hisanaga, M. Goedert, M. Hasegawa, Cysteine misincorporation in bacterially expressed human alpha-synuclein, FEBS Lett, 580 (2006) 1775-1779.
- [64] M. Kurosawa, G. Matsumoto, Y. Kino, M. Okuno, M. Kurosawa-Yamada, C. Washizu, H. Taniguchi, K. Nakaso, T. Yanagawa, E. Warabi, T. Shimogori, T. Sakurai, N. Hattori, N. Nukina, Depletion of p62 reduces nuclear inclusions and paradoxically ameliorates disease phenotypes in Huntington's model mice, Hum Mol Genet, 24 (2015) 1092-1105.
- [65] A. Iwata, S. Miura, I. Kanazawa, M. Sawada, N. Nukina, alpha-Synuclein forms a complex with transcription factor Elk-1, J Neurochem, 77 (2001) 239-252.
- [66] Y. Ohhashi, Y. Yamaguchi, H. Kurahashi, Y.O. Kamatari, S. Sugiyama, B. Uluca, T. Piechatzek, Y. Komi, T. Shida, H. Muller, S. Hanashima, H. Heise, K. Kuwata, M. Tanaka, Molecular basis for diversification of yeast prion strain conformation, Proc Natl Acad Sci U

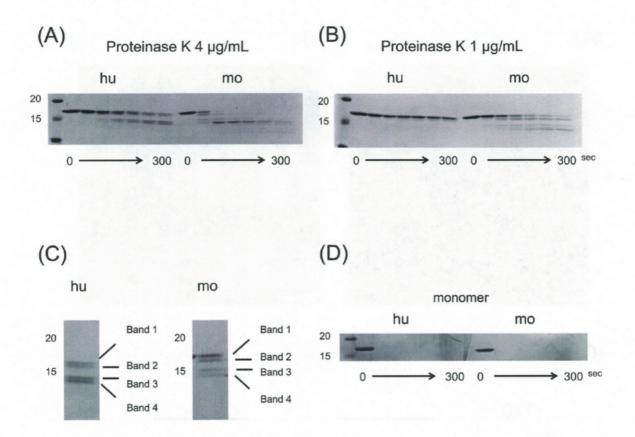
- S A, 115 (2018) 2389-2394.
- [67] H. Heise, W. Hoyer, S. Becker, O.C. Andronesi, D. Riedel, M. Baldus, Molecular-level secondary structure, polymorphism, and dynamics of full-length alpha-synuclein fibrils studied by solid-state NMR, Proc Natl Acad Sci U S A, 102 (2005) 15871-15876.
- [68] G. Lv, A. Kumar, K. Giller, M.L. Orcellet, D. Riedel, C.O. Fernandez, S. Becker, A. Lange, Structural comparison of mouse and human alpha-synuclein amyloid fibrils by solid-state NMR, J Mol Biol, 420 (2012) 99-111.
- [69] Y. Furukawa, K. Kaneko, N. Nukina, Tau protein assembles into isoform- and disulfide-dependent polymorphic fibrils with distinct structural properties, J Biol Chem, 286 (2011) 27236-27246.
- [70] Y. Furukawa, K. Kaneko, K. Yamanaka, N. Nukina, Mutation-dependent polymorphism of Cu,Zn-superoxide dismutase aggregates in the familial form of amyotrophic lateral sclerosis, J Biol Chem, 285 (2010) 22221-22231.
- [71] A. Weiss, C. Klein, B. Woodman, K. Sathasivam, M. Bibel, E. Regulier, G.P. Bates, P. Paganetti, Sensitive biochemical aggregate detection reveals aggregation onset before symptom development in cellular and murine models of Huntington's disease, J Neurochem, 104 (2008) 846-858.
- [72] R. Melki, Role of Different Alpha-Synuclein Strains in Synucleinopathies, Similarities with other Neurodegenerative Diseases, J Parkinsons Dis, 5 (2015) 217-227.
- [73] M.K. Lee, W. Stirling, Y. Xu, X. Xu, D. Qui, A.S. Mandir, T.M. Dawson, N.G. Copeland, N.A. Jenkins, D.L. Price, Human alpha-synuclein-harboring familial Parkinson's disease-linked Ala-53 --> Thr mutation causes neurodegenerative disease with alpha-synuclein aggregation in transgenic mice, Proc Natl Acad Sci U S A, 99 (2002) 8968-8973.
- [74] R. Tycko, Amyloid polymorphism: structural basis and neurobiological relevance, Neuron, 86 (2015) 632-645.
- [75] H. Miake, H. Mizusawa, T. Iwatsubo, M. Hasegawa, Biochemical characterization of the core structure of alpha-synuclein filaments, J Biol Chem, 277 (2002) 19213-19219.
- [76] K.R. Kumar, K. Lohmann, C. Klein, Genetics of Parkinson disease and other movement disorders, Curr Opin Neurol, 25 (2012) 466-474.
- [77] A.P. Kiely, Y.T. Asi, E. Kara, P. Limousin, H. Ling, P. Lewis, C. Proukakis, N. Quinn, A.J. Lees, J. Hardy, T. Revesz, H. Houlden, J.L. Holton, alpha-Synucleinopathy associated with G51D SNCA mutation: a link between Parkinson's disease and multiple system atrophy?, Acta Neuropathol, 125 (2013) 753-769.
- [78] A.P. Kiely, H. Ling, Y.T. Asi, E. Kara, C. Proukakis, A.H. Schapira, H.R. Morris, H.C.

- Roberts, S. Lubbe, P. Limousin, P.A. Lewis, A.J. Lees, N. Quinn, J. Hardy, S. Love, T. Revesz, H. Houlden, J.L. Holton, Distinct clinical and neuropathological features of G51D SNCA mutation cases compared with SNCA duplication and H50Q mutation, Mol Neurodegener, 10 (2015) 41.
- [79] W. Choi, S. Zibaee, R. Jakes, L.C. Serpell, B. Davletov, R.A. Crowther, M. Goedert, Mutation E46K increases phospholipid binding and assembly into filaments of human alpha-synuclein, FEBS Lett, 576 (2004) 363-368.
- [80] L.C. Serpell, J. Berriman, R. Jakes, M. Goedert, R.A. Crowther, Fiber diffraction of synthetic alpha-synuclein filaments shows amyloid-like cross-beta conformation, Proc Natl Acad Sci U S A, 97 (2000) 4897-4902.
- [81] N.J. Rutherford, B.D. Moore, T.E. Golde, B.I. Giasson, Divergent effects of the H50Q and G51D SNCA mutations on the aggregation of alpha-synuclein, J Neurochem, 131 (2014) 859-867.
- [82] D.F. Lazaro, M.C. Dias, A. Carija, S. Navarro, C.S. Madaleno, S. Tenreiro, S. Ventura, T.F. Outeiro, The effects of the novel A53E alpha-synuclein mutation on its oligomerization and aggregation, Acta Neuropathol Commun, 4 (2016) 128.
- [83] O. Khalaf, B. Fauvet, A. Oueslati, I. Dikiy, A.L. Mahul-Mellier, F.S. Ruggeri, M.K. Mbefo, F. Vercruysse, G. Dietler, S.J. Lee, D. Eliezer, H.A. Lashuel, The H50Q mutation enhances alpha-synuclein aggregation, secretion, and toxicity, J Biol Chem, 289 (2014) 21856-21876.
- [84] S. Taniguchi-Watanabe, T. Arai, F. Kametani, T. Nonaka, M. Masuda-Suzukake, A. Tarutani, S. Murayama, Y. Saito, K. Arima, M. Yoshida, H. Akiyama, A. Robinson, D.M.A. Mann, T. Iwatsubo, M. Hasegawa, Biochemical classification of tauopathies by immunoblot, protein sequence and mass spectrometric analyses of sarkosyl-insoluble and trypsin-resistant tau, Acta Neuropathol, 131 (2016) 267-280.



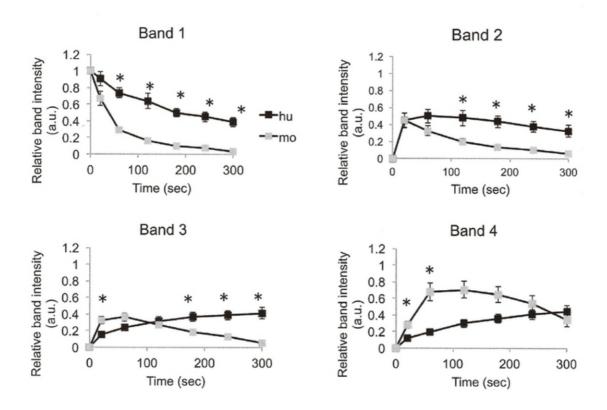
Supplementary Fig. S1 Homogeneity of human and mouse alpha-synuclein fibrils

Representative electron micrographs of (A) human WT and (B) mouse a-syn fibrils are shown. Scale bars indicate 200 nm. The number of fibrils from each electron micrograph are shown using means from three different field of view (N=3). The homogeneity of human and mouse a-syn fibrils is 100% and 97.52%, respectively. Data are shown as means \pm SE.



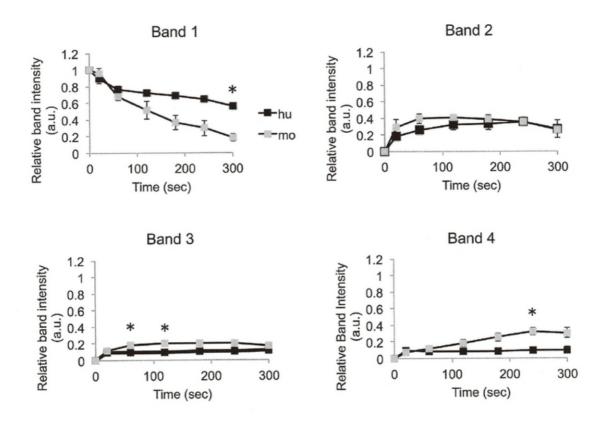
Supplementary Fig. S2 The digestion patterns with proteinase K of human and mouse alpha-synuclein fibrils in detail

The digestion patterns of human and mouse alpha-synuclein are shown using different concentration of proteinase K: (A) (4 μ g/mL) and (B) (1 μ g/mL). Samples were collected at each time point (20, 60, 120, 180, 240, and 300 s). (C) The digested bands at 300 s (human) and 20 s (mouse) are shown. Four bands were detected in this experiment. (D) Differences in the digestion patterns with proteinase K cannot be detected in the monomer states of human and mouse a-syn. Numbers on the left indicate molecular weight. "0" indicates pre-digested samples; "300" indicates proteinase K reaction time (in seconds).



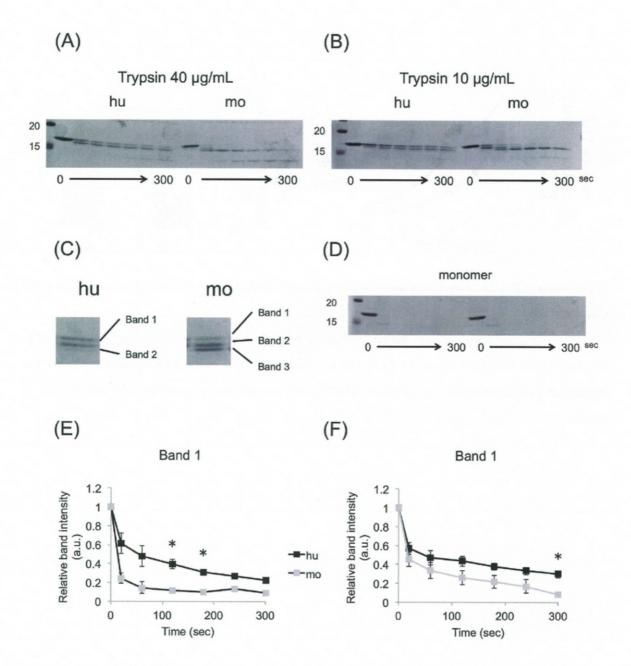
Supplementary Fig. S3 The quantification of digestion patterns of human and mouse a-syn fibrils using proteinase \mathbf{K}

The detected 4 bands digested with proteinase K (4 μ g/mL) were quantified using ImageJ. The data are normalized by the respective 0 time-point (pre-reaction) sample. Means and standard errors of replicates (n = 5) are shown. Asterisks indicates statistically significant difference based on P < 0.05.



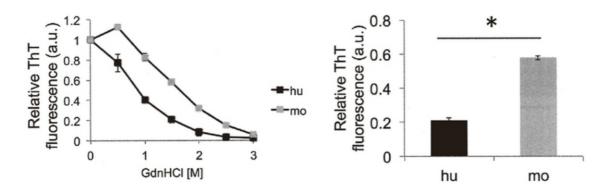
 $Supplementary \ Fig. \ S4 \ The \ quantification \ of \ digestion \ patterns \ of \ human \ and \ mouse \ a-syn \ fibrils \ using \\ proteinase \ K$

The detected bands digested with proteinase K (1 μ g/mL) were quantified using ImageJ. The data are normalized by the respective 0 time-point (pre-reaction) sample. Means and standard errors of replicates (n = 3) are shown. Asterisks indicates statistically significant difference based on P < 0.05.



Supplementary Fig. S5 The digestion patterns with trypsin of human and mouse alpha-synuclein fibrils in detail

(A, B) The digestion patterns of human and mouse a-syn are shown using different concentration of trypsin (40 μ g/mL) and (10 μ g/mL). (C) The digested bands at 300 s (human) and 20 s (mouse) are shown. (D) These differences in the digestion patterns with trypsin can cannot be detected in the monomer states of human and mouse a-syn. Numbers on the left indicate molecular weight. "0" indicates pre-digested samples; "300" indicates trypsin reaction time (in seconds). (E, F) The 1st bands digested with trypsin 40 μ g/mL and 10 μ g/mL were quantified. Means and standard errors of replicates (n = 3) are shown. Asterisks indicates statistically significant difference based on P < 0.05.



Supplementary Fig. S6 Human and mouse alpha-synuclein showed distinct denaturation resistance from Gdn-HCl

GdnHCl-denaturation assay indicates distinct biochemical properties of human WT and mouse alpha-synuclein. (B) Aggregation was quantified at 1.5 M GdnHCl in human WT and mouse alpha-synucleins. Means and standard errors of replicates (n = 3) are shown. Asterisks indicates statistically significant difference based on P < 0.05.